Atmos. Chem. Phys. Discuss., 12, 29801–29849, 2012
www.atmos-chem-phys-discuss.net/12/29801/2012/
doi:10.5194/acpd-12-29801-2012

Atmospheric Chemistry and Physics Discussions

Impact of the aging process of black carbon aerosols on their spatial distribution, hygroscopicity, and radiative forcing in a global climate model

D. Goto[1], N. Oshima[2], T. Nakajima[3], T. Takemura[4], and T. Ohara[1]

[1]National Institute for Environmental Studies, Ibaraki, Japan
[2]Meteorological Research Institute, Ibaraki, Japan
[3]Atmosphere and Ocean Research Institute, The University of Tokyo, Chiba, Japan
[4]Research Institute for Applied Mechanics, Kyusyu University, Fukuoka, Japan

Received: 26 October 2012 – Accepted: 14 November 2012 – Published: 20 November 2012

Correspondence to: D. Goto (goto.daisuke@nies.go.jp)

Published by Copernicus Publications on behalf of the European Geosciences Union.

Abstract

Black carbon (BC) absorbs shortwave radiation more strongly than any other type of aerosol, and an accurate simulation of the aging processes of BC-containing particle is required to properly predict aerosol radiative forcing (ARF) and climate change. However, BC aging processes have been simplified in general circulation models (GCMs) due to limited computational resources. In particular, differences in the representation of the mixing states of BC-containing particles between GCMs constitute one of main reasons for the uncertainty in ARF estimates. To understand an impact of the BC aging processes and the mixing state of BC on the spatial distribution of BC and ARF caused by BC (BC-ARF), we implemented three different methods of incorporating BC aging processes into a global aerosol transport model, SPRINTARS: (1) the "AGV" method, using variable conversion rates of BC aging based on a new type of parameterization depending on both BC amount and sulfuric acid; (2) the "AGF" method, using a constant conversion rate used worldwide in GCMs; and (3) the "ORIG" method, which is used in the original SPRINTARS. First, we found that these different methods produced different BC burden within 10 % over industrial areas and 50 % over remote oceans. Second, a ratio of water-insoluble BC to total BC (WIBC ratio) was very different among the three methods. Near the BC source region, for example, the WIBC ratios were estimated to be 80–90 % (AGV and AGF) and 50–60 % (ORIG). Third, although the BC aging process in GCMs had small impacts on the BC burden, they had a large impact on BC-ARF through a change in both the WIBC ratio and non-BC compounds coating on BC cores. As a result, possible differences in the treatment of the BC aging process between aerosol modeling studies can produce a difference of approximately 0.3 Wm^{-2} in the magnitude of BC-ARF, which is comparable to the uncertainty suggested by results from a global aerosol modeling intercomparison project, AeroCom. The surface aerosol forcing efficiencies normalized by aerosol optical thickness and by BC burden varied greatly with region in the AGV method, which allowed for the existence of internally mixed BC and sulfate, whereas these were not varied with region in

ACPD

12, 29801–29849, 2012

the AGF method. These results suggest that the efficiencies of BC-ARF obtained by previous studies using the AGF method are significantly underestimated.

1 Introduction

Black carbon (BC) strongly absorbs shortwave radiation and thus have a more significant influence on radiative perturbations than other aerosol components (Hansen et al., 1997; Jacobson, 2002; Forster et al., 2007). Estimates of the radiative impacts of BC aerosols due to the aerosol direct effect caused by fossil fuel BC and biomass burning are still very uncertain, with reported positive forcings of $+0.20 \pm 0.15$ and $+0.03 \pm 0.12\,\mathrm{W\,m^{-2}}$, respectively (Forster et al., 2007). BC can also affect radiative fluxes through a semi-direct radiative forcing by promoting the evaporation of clouds (e.g. Hansen et al., 1997), through the deposition effect on snow (e.g. Flanner et al., 2007) and through indirect radiative forcings by modulating the cloud microphysics and the precipitation rate (e.g. Menon et al., 2002). The uncertainty in these radiative effects of BC may be due to uncertainties in both the spatial distribution of BC, which is determined by various atmospheric processes, such as emission, transport, chemical transposition, and deposition processes (Schulz et al., 2006; Koch et al., 2009; Shindell et al., 2008; Liu et al., 2011; Oshima et al., 2012), and the optical properties of BC (Jacobson, 2002; Bond and Bergstrom, 2006). These properties depend on the particle size distribution, hygroscopicity, mixing state of the particles, and refractive index of BC.

BC particles are emitted from, for example, an incomplete combustion of fossil fuels, biofuels, and biomass burning. Fresh BC particles, which are composed of hydrophobic or water-insoluble BC (hereafter called WIBC), are generally more pure and bare than aged BC particles (Weingartner et al., 1997). In the atmosphere, fresh BC particles become internally mixed with other aerosol components through condensation, coagulation, cloud processing, and photochemical oxidation processes (e.g. Seinfeld and Pandis, 2006). These processes are called “BC aging processes”, which generally

ACPD
12, 29801–29849, 2012

yield hydrophilic or water-soluble BC (hereafter called WSBC). Many measurements suggest that atmospheric BC particles are often internally mixed with other aerosol species, such as sulfate and organic compounds (Okada, 1985; Katrinak et al., 1992; Parungo et al. 1994; Pósfai et al., 1999; Guazzotti et al., 2001; Naoe and Okada, 2001; Clarke et al., 2004; Johnson et al., 2005; Schwarz et al., 2006, 2008; Moteki et al., 2007; Shiraiwa et al., 2008; Adachi and Buseck, 2008; Moffet and Prather, 2009; McMeeking et al., 2010; Pósfai and Buseck, 2010; Takahama et al., 2010; Pratt and Prather, 2010). However, most global models cannot fully take these internally mixed particles into account because of the large amount of CPU time required to do so. Such a large amount of CPU time is not typically suitable for the prediction of climate change using general circulation models (GCMs) or atmosphere-ocean coupled GCMs, although some global aerosol transport models do take into account the internal mixing and related processes (Jacobson, 2003; Stier et al., 2005; Pierce et al., 2007; Bauer et al., 2008). To date, most global aerosol transport models take into account both WIBC and WSBC (Takemura et al., 2005; Kim et al., 2008; Liu et al., 2011), while some models take into account only WSBC for simplicity (Liao et al., 2004; Zhang et al., 2004; Fast et al., 2006; Zaveri et al., 2008). In addition, in the former type of model, WSBC is often considered by ignoring condensed compounds in BC, which become light-absorbing in BC-containing particles (e.g. Chin et al., 2002, 2009; Park et al., 2003; Reddy and Boucher, 2004; Easter et al., 2004; Bellouin et al., 2007; Myhre et al., 2009). Differences in the mixing state of WSBC particles can directly affect optical properties of these particles and indirectly affect their spatial distribution by modifying their removal efficiencies. This fact means that a difference in the ratios of the number of WIBC, WSBC, and non-BC-containing particles to the total amount of BC in the atmosphere and a ratio of the amount of BC to other compounds inside one particle can critically alter estimations in the aerosol direct radiative forcing due to BC aerosols (BC-ARF). Indeed, these differences could produce uncertainty in BC-ARF calculated using nine global aerosol-transport models participated in an international model-comparison project, AeroCom (Schulz et al., 2006).

ACPD
12, 29801–29849, 2012

The mixing state of BC with other compounds in an aerosol transport model is determined by the BC aging process. Ideally, this process should be calculated by taking into account aerosol dynamics, i.e. condensation and coagulation, using a size-resolved aerosol representation, such as was in the simulations performed by Jacobson (2003), Liu et al. (2005), and Stier et al. (2005). However, these explicit calculations are computationally expensive with regard to performing global climate calculations. A parameterization, therefore, is very useful and powerful for describing the BC aging process in global climate models. In fact, global aerosol transport models treat simplified BC aging processes using a conversion rate (τ_{BC}) between WIBC and WSBC in the atmosphere with a range of one to two days without taking into account any existence of condensed matter in core BC particles (e.g. Cooke and Wilson, 1996; Wilson et al., 2001; Chin et al., 2002; Chung and Seinfeld, 2002; Park et al., 2003; Reddy and Boucher, 2004; Koch and Hansen, 2005; Croft et al., 2005; Liu et al., 2011). Other models, such as the model reported by Takemura et al. (2005), assume that the BC aging processes occur within one grid and one time step in the GCM and that not only WIBC but also WSBC is emitted from combustion processes. Recently, the BC aging process has been parameterized using physically based methods (Riemer et al., 2004, 2009; Croft et al., 2005; Liu et al., 2011; Oshima and Koike, 2012).

In global BC simulations, previous studies compared BC spatial distributions among various parameterizations of the BC aging process (Croft et al., 2005; Vignati et al., 2010; Liu et al., 2011). As far as we know, Croft et al. (2005) investigated differences in the BC burden between different BC aging parameterizations for the first time. Furthermore, Vignati et al. (2010) compared results obtained by the traditional parameterization using a fixed τ_{BC} with results obtained by a sophisticated treatment of the BC aging process including aerosol dynamic processes. They found that the differences in the BC burden between the two modules are very small over BC source regions, whereas the differences are large over remote areas. However, these previous studies did not address an impact of aerosol optical properties on radiative forcings.

ACPD
12, 29801–29849, 2012

Therefore, in this study, we addressed the impact of the difference in the treatment of the BC aging process on BC spatial distributions and, thus, BC-ARF. In particular, we quantified the difference in BC-ARF between the most widely used method and other methods to estimate the differences in BC-ARF among AeroCom models. To this end, we performed numerical experiments using a global aerosol-radiation transport model, SPRINTARS, developed by Takemura et al. (2005) and Goto et al. (2011a) and participated in the AeroCom project using three different methods for addressing the BC aging processes: (1) a method using a variable τ_{BC} calculated by a parameterization, which is based on the method of spectral binning of BC aerosols developed by Oshima and Koike (2012) (hereafter referred to as the "AGV" method); (2) a traditional method using the constant τ_{BC}, which is widely used in other GCMs (hereafter referred to as the "AGF" method); and (3) the method used in the original SPRINTARS (hereafter referred to as the "ORIG" method). The algorithms used in these methods are discussed in Sect. 2. BC simulations carried out by comparing modeling results with observations are presented in Sect. 3. The radiative impacts of BC particles are discussed in Sect. 4. Finally, we present our conclusions in Sect. 5.

2 Model description

2.1 Global aerosol transport-radiation model (SPRINTARS)

We used the Spectral Radiation-Transport Model for Aerosol Species (SPRINTARS), which is a global three-dimensional aerosol transport radiation model, developed by Takemura et al. (2000, 2002, 2005, 2009) and Goto et al. (2011a, b, c). The SPRINTARS model has been implemented in an atmospheric general circulation model (AGCM), named "MIROC (Model for Interdisciplinary Research on Climate)", developed by the University of Tokyo, National Institute for Environmental Studies (NIES), and the Japan Agency for Marine-Earth and Technology (JAMSTEC) and used for global climate modeling (K-1 Developers, 2004; Watanabe et al., 2010).

ACPD
12, 29801–29849, 2012

The SPRINTARS model calculates the mass mixing ratios of the main tropospheric aerosols, i.e. carbonaceous aerosol (BC; POA, primary organic aerosol; BSOA, biogenic secondary organic aerosol), sulfate, soil dust, sea salt, and the precursor gases of sulfate, i.e. SO_2 and dimethylsulfide. The aerosol module accounts for various processes, such as emission, advection, diffusion, sulfur chemistry, wet deposition and dry deposition including gravitational settling.

The emission inventories considered in the present study were described by Goto et al. (2011a, c), where the anthropogenic SO_2 and BC emission flux in 2003 used in this study is based on the EMEP emission inventory (http://webdab.emep.int/) over Europe, the results of Streets et al. (2003) over Asia, and the results of Takemura et al. (2005) in the other regions. As a result, the global mean BC emission amount from anthropogenic sources excluding biomass burning is estimated to be $11.4\,\mathrm{Tg\,yr^{-1}}$, which may be higher than the mean of $11.9 \pm 1.4\,\mathrm{Tg\,yr^{-1}}$ used in the AeroCom Phase I model (Textor et al., 2006) and the mean of $4.4\,\mathrm{Tg\,yr^{-1}}$ used in Bond et al. (2007). Goto et al. (2011c) used the same BC emission inventory used in the present study and showed that the simulated BC concentrations over India were closer to the observed concentrations than the results obtained using emission inventories used in the AeroCom model. Biomass burning emissions for each day in 2003 are based on the fire maps derived from both MODIS (Davies et al., 2009) and GFED version 2 (Randerson et al., 2006). The global mean BC emission amount is estimated to be $2.6\,\mathrm{Tg\,yr^{-1}}$ in both the present study and in that by Bond et al. (2007).

The model results were calculated under the year 2003 conditions using monthly averaged global distributions for sea surface temperature and sea ice, which had been re-analyzed by the Hadley Centre, UK Met Office. Meteorological fields (wind, water vapor, and temperature) were nudged from the NCAR/NCEP reanalysis data. The spatial and vertical resolutions were set to the T42 resolution, i.e. $2.8^\circ \times 2.8^\circ$ (ca. 300 km by 300 km) and 20 layers.

ACPD
12, 29801–29849, 2012

2.2 Treatment of BC particles in a global aerosol transport model

We investigated three types of the BC aging processes using the global aerosol transport model SPRINTARS, as shown in Table 1. The first method is similar to the second, but in the former, τ_{BC} is variable (the "AGV" method). The second method is widely used in most global models with a fixed τ_{BC} (the "AGF" method). The third method is used in the original SPRINTARS model (the "ORIG" method).

2.2.1 BC aging method with a variable or fixed conversion rate (AGV and AGF)

The BC aging processes in the atmosphere are expressed as the conversion rate or τ_{BC} from WIBC to WSBC. The change in WIBC concentration in the time t can be written by using τ_{BC} as follows:

$$[\mathrm{WIBC}](t) = [\mathrm{WIBC}](t-1) + [\mathrm{WIBC}](t-1) \times \exp\left(-\frac{t}{\tau_{BC}}\right), \quad (1)$$

$$[\mathrm{WSBC}](t) = [\mathrm{WSBC}](t-1) + [\mathrm{WIBC}](t-1) \times \left(1 - \exp\left(-\frac{t}{\tau_{BC}}\right)\right), \quad (2)$$

where [WIBC] and [WSBC] are the concentrations of WIBC and WSBC, respectively. As we mentioned in Sect. 1, τ_{BC} is often fixed to a range of 1 to 1.2 days (e.g. Chung and Seinfeld, 2002; Chin et al., 2002). This fixation of τ_{BC} corresponds to the second method, i.e. the AGF method, used in this study. However, τ_{BC} can be changed under various conditions, depending on a number concentration of particles to be aged and a concentration of condensed gases. Recently, Oshima and Koike (2012) developed a parameterization of the BC aging process using a detailed physics-based aerosol mixing state resolved box model (Oshima et al., 2009a, b). They represented the BC aging process using a variable τ_{BC} value as follows:

$$\tau_{BC} = \frac{a}{v_c}, \quad (3)$$

ACPD
12, 29801–29849, 2012

$$v_c = \frac{\partial m_{BC}}{\partial t} \frac{1}{[WIBC]}, \quad (4)$$

$$\frac{\partial m_{BC}}{\partial t} = \frac{N_{WIBC}}{N_{tot}} [H_2SO_4] \frac{60 \times 60}{dt\,(s)}, \quad (5)$$

where a is 0.375 under the assumed BC particle radius of 87.5 nm and v_c is the coating rate of BC normalized by the BC mass concentration per hour. $[H_2SO_4]$ is the sulfuric acid concentration. N_{WIBC} and N_{tot} are the particle number concentrations of WIBC and total aerosols, respectively. The term dt is the time step of the SPRINTARS model under T42 resolution in units of seconds. We call this method the "Aging-Variable", i.e. "AGV", method in this study. τ_{BC} depends on the concentration of sulfuric acid, which is formed from the photo-oxidation of SO_2 by OH radicals; thus, the variation in τ_{BC} has a minimum during the daytime and a maximum during the night. This parameterization only treats the condensational growth of BC and does not treat other BC aging processes, such as coagulation (Oshima and Koike, 2012). Therefore, we set the maximum of τ_{BC} to be 20 days following Liu et al. (2011).

Furthermore, in the AGV method, we can prognosticate the change in the concentration of sulfate contained in WSBC particles at time t after sulfuric acid is condensed in WSBC particles as follows:

$$[SO_4](t) = [SO_4](t-1) + b \times [H_2SO_4]_{SO_2} + OH \times \frac{N_{BC}}{N_{tot}}, \quad (6)$$

where b and $[H_2\ SO_4]_{SO_2+OH}$ represent a unit conversion factor and the concentration of sulfuric acid formed from SO_2 oxidation by OH radicals within the time step dt, respectively. N_{BC} is the particle number concentrations of total BC. Therefore, the AGV method treats four tracers related to carbonaceous particles, OC, WIBC, WSBC, and

ACPD
12, 29801–29849, 2012

sulfate in WSBC, whereas the AGF method treats only three tracers of carbonaceous particles, namely OC, WIBC and WSBC (see Table 1).

In addition to using the ORIG method reported by Takemura et al. (2005), we upgraded the information regarding BC properties using recent observations. In the AGV and AGF methods, WIBC refers to pure BC particles without any hygroscopic growth and with a center radius of 92.5 nm in the mass size distribution, as suggested by in-situ measurements (Schwarz et al., 2006; Moteki et al., 2007; Shiwaiwa et al., 2008; McMeeking et al., 2010). A WSBC particle often has a BC core, with a shell-to-core volume ratio of approximately 1.2 (Shiwaiwa et al., 2008); therefore, we assumed that the center radius of WSBC particles is 110 nm. The standard deviation of the WSBC particles was set to 1.53, as suggested by Omar et al. (2005) and Moteki et al. (2007). The particle hygroscopicity of WSBC was the same as that used for particles in pure sulfate by Takemura et al. (2002). The density of the BC compounds was set to 1.8 g cm^{-3}, as suggested by measurements (e.g. McMeeking et al., 2010). In the AGV and AGF methods, the WIBC and WSBC compounds constituted 80 and 20 % of the total BC emission in all sources, respectively, as indicated by previous studies (e.g. Chin et al., 2002).

2.2.2 Original method in the SPRINTARS model (ORIG)

In the original SPRINTARS, WIBC and WSBC are considerd, although WIBC is not converted to WSBC in the atmosphere. With regard to BC-containing particles, BC aerosols are categorized into three types: pure BC (i.e. WIBC) and two types of WSBC (the ratios of BC to OC were set to be 6.67 and 3.33). In Takemura et al. (2002), WIBC has a lognormal size distribution with a mode radius of 11.8 nm, whereas the two types of WSBC have lognormal size distributions with mode radii of 100 nm. The standard deviations of the WIBC and WSBC particles were set to 2.00, as suggested by Hess et al. (1998). The particle hygroscopicity of WSBC is the same as that used for pure OC by Takemura et al. (2002) and Goto et al. (2011a). The density of WSBC was set to 1.25 g cm^{-3}, as in Takemura et al. (2002). In the original SPRINTARS model,

ACPD
12, 29801–29849, 2012

researchers assume that a half of the BC compound emitted from fossil fuel combustion is externally mixed with other species (i.e. WIBC), whereas other BC compounds emitted from biomass burning, agricultural activities and biofuel combustion are internally mixed with OC (i.e. WSBCs) within one GCM time step (ca. 20 min) and one grid (ca. 300 km by 300 km).

2.2.3 BC deposition process

Deposition processes of the BC include both wet (through both rainout and washout) and dry (by both turbulence and gravity) deposition. The rainout represents the process through which aerosol compounds in a cloud droplet are scavenged by precipitation after aerosol activation in the cloud droplet. The interstitial fractions of WSBC and WIBC were fixed to 0.9 and 0.1, respectively. The washout process, i.e. the process through which aerosols in the atmosphere (not in clouds) are scavenged through collision with raindrops, and dry deposition by turbulence and gravity are also considered as they were by Takemura et al. (2002). That means that in all of the methods (AGV, AGF, and ORIG), we treated these deposition processes for BC aerosols in the same manner as that described by Takemura et al. (2002).

2.3 Optical and radiative calculation

Radiation transfer with a k-distribution scheme, MSTRN-8, coupled online to AGCM can handle scattering, absorption, and emission by aerosol and cloud particles, as well as absorption by gaseous constituents, and can be used to calculate the aerosol direct and indirect effects (Nakajima et al., 2000; Sekiguchi and Nakajima, 2008). We calculated aerosol optical properties (aerosol optical thickness, or AOT, and absorption aerosol optical thickness, or AAOT) using the same Mie theory methods used by Goto et al. (2011a, b, c). Optical calculations for WSBC are based on Mie theory, where the refractive indices of chemical compounds are replaced by volume-weighted refractive indices under the assumption of complete internal mixture due to full coupling to

ACPD
12, 29801–29849, 2012

our radiation code. This simplicity may create errors in AOT within ranges of < 10 and < 5 % over Asia, as suggested by Goto et al. (2011b). The aerosol optical properties estimated in the present study by using complete internal mixture may have been overestimated compared with those calculated using core-shell mixing, as suggested by Jacobson (2001); however, the objectives of the present study were to estimate the differences in the BC burden and BC-ARF among various numerical experiments by considering different BC aging processes.

The extinction and absorption coefficients, which are determined by Mie theory based on particle size distribution (its size center and width), particle density, refractive index, hygroscopicity, and wavelength, of BC particles are shown in Fig. 1. The aerosol optical properties considered in the AGV and AGF methods were mostly up to date in the present study, whereas those considered in the ORIG method were identical to those used by Takemura et al. (2002, 2005). In the AGF and AGV methods, we changed the size distribution and density of WIBC and WSBC, as mentioned in the previous section. The refractive index of pure BC was set to 1.95–0.79i, as proposed by Bond and Bergstrom (2006), which has recently estimated larger absorption. As a result, in the AGV and AGF methods, the extinction coefficients of BC containing particle distributions at a wavelength of 550 nm were calculated to be 9.2 (for WIBC), 6.6 (for WSBC under dry conditions), and 15.0 $m^2\,g^{-1}$ (for WSBC under wet conditions, i.e. 90 % RH). The absorption coefficients of BC at a wavelength of 550 nm were calculated to be 6.2 (for WIBC), 4.3 (for WSBC under dry conditions), and 6.0 $m^2\,g^{-1}$ (for WSBC under wet conditions, i.e. 90 % RH). In the ORIG method, by contrast, the refractive index of pure BC was set to 1.75–0.44i, as proposed by Hess et al. (1998) and still widely used in aerosol modeling studies. The extinction coefficients of BC at a wavelength of 550 nm were calculated to be 8.3 (for WIBC) and 4.5 to 5.0 (for WSBC under dry conditions) and 20.0 to 21.4 m^2g^{-1} (for WSBC under wet conditions, i.e. 90 % RH), whereas the absorption coefficients of BC at a wavelength of 550 nm were calculated to be 6.5 (for WIBC), 0.8 to 1.0 (for WSBC under dry conditions), and 1.2 to 1.5 m^2g^{-1} (for WSBC under wet conditions, i.e. 90 % RH). In addition, although these absorption

ACPD
12, 29801–29849, 2012

values for WIBC in all experiments (AGV, AGF, and ORIG methods) are near the lower limit of the range estimated by Bond and Bergstrom (2006) and Clarke et al. (2004) under dry conditions, these values under wet conditions are different between the two aging methods (AGV and AGF) and the ORIG method due to differences in mixing fraction, chemical compounds, size distribution, density, and hygroscopicity.

BC-ARF is calculated as a difference in net fluxes with and without BC compounds under the same meteorological conditions, as in the method of Takemura et al. (2005) and Goto et al. (2008). Therefore, in the experiment without BC compounds, all OC aerosols in the ORIG method were pure OC and all sulfate components in the AGV method were pure sulfate. These models can also calculate the radiative forcing under clear-sky and all-sky conditions at any vertical levels.

3 Results

3.1 BC bulk amount

Figure 2 and Table 2 show the annual average BC mass concentrations near the surface as observed and simulated in this study over the United States, Europe, China, India, and other Asian countries. The observations made in 2003 were limited, except for those over the United States (IMPROVE) and Europe (EMEP); therefore, we used the dataset in 2006 over China (Zhang et al., 2008) and during 2000–2008 over India (Goto et al., 2011c) and other Asian countries (Tokyo/Japan by Kondo et al., 2006 and Minoura et al., 2006; Rishiri/Japan by Matsumoto et al., 2007; Incheon/Korea by Kim et al., 2006; Seoul/Korea by Kim et al., 2007; Tomsk/Russia by Kozlov et al., 2008; Phimai/Thailand by H. Tsuruta, 2011, personal communication). These observations show that among these industrial regions, the United States has the lowest BC mass concentration, with the mean ranging mostly from 0.1 to 1 $\mu g\,m^{-3}$, and Asia has the highest BC, with concentrations of up to 10 $\mu g\,m^{-3}$. In the present study, however, the simulated BC mass concentration over the United States reached 2 $\mu g\,m^{-3}$.

ACPD
12, 29801–29849, 2012

Furthermore, the simulated BC concentration over the United States was higher than that over Europe, which is the reverse tendency indicated by the observations. This simulation result may be caused by an uncertainty in the BC emission inventory over the United States because the BC emission inventories over Europe and Asia were interpolated using sophisticated regional inventories. Over the remote areas shown in Fig. 3, the use of different BC aging processes yielded a factor of 10 differences in the simulated BC surface mass concentration near polar sites (Barrow, Zeppelin, Alert and Halley). However, except for Amsterdam Island and Zeppelin, the difference in the BC mass concentration between the observations and the simulations was large and thus cannot be explained by only differences in the BC aging process in the present study.

The horizontal distribution of the annually averaged BC mass concentration at the surface calculated according to the AGV method is shown in Fig. 4a. This BC concentration represents the sum of the concentrations of both WIBC and WSBC compounds. In Fig. 4b and c, the differences in the BC mass concentration among the experiments are estimated to be at most 10 % near aerosol sources (the United State, Europe, and Asia) and at most 50 % over remote areas (Fig. 4b and c). The pattern of the relative difference between the AGV and AGF methods is quite different from that between the AGV and ORIG methods. Along the outflow of BC air masses from industrial regions to remote areas, the BC mass concentration simulated by the AGV method becomes larger than that simulated by the AGF method and smaller than that simulated by the ORIG method. Over remote oceans, the magnitude of the difference in the BC mass concentration between the AGV and ORIG methods reaches 50 %. In addition, over the African coast, where biomass burning affects the air quality, the BC mass concentration simulated by the AGV method is larger than the concentrations simulated by both the AGF and ORIG methods by 10 and 20 %, respectively. Even though we can find differences in the simulated BC mass concentration among methods, the surface BC mass concentrations calculated in the present study are fully within the uncertainty range of the AeroCom models shown in Koch et al. (2009).

ACPD
12, 29801–29849, 2012

To understand the vertical transport patterns in our model, we compared annual and zonal mean BC mass concentrations, as shown in Fig. 5. The simulated BC mass concentrations ranging from 0.05 to 0.1 $\mu g\,m^{-3}$ over the latitudes ranging from 15° N to 15° S lie at a sigma level of 0.5 to 0.6 in all simulations in the present study. The levels are almost comparable to those obtained by Vignati et al. (2010) and Koch et al. (2009), who compared their simulated BC concentrations with those observed during a flight campaign over the Arctic during spring and summer in 2008 under ARCTAS procejt. The largest differences in the simulated BC concentrations between the present simulations are found for locations above the equator, with annual averages differing by at most 0.05 $\mu g\,m^{-3}$.

Figure 6 shows the annual mean column BC concentrations simulated in this study. The global mean values are estimated to be 0.26 Tg, which is slightly higher than the values reported in the AeroCom study by Textor et al. (2006), who indicated average values of 0.24 ± 0.05 Tg; this discrepancy is due to the higher BC emission amount in this study, as discussed in Sect. 2. The BC burden calculated by the AGV method is higher than that calculated by the AGF method, with the relative difference ranging from −1 to +5 % over industrial areas and from 10 to 50 % over other regions, including remote areas. In addition, the BC burden calculated by the AGV method is also higher over biomass burning regions than that calculated by the ORIG method, with the difference ranging from −1 to +20 %; meanwhile, the BC burden calculated by the AGV method is smaller over other regions, including industrial regions and remote oceans, with the difference reaching up to −50 %.

Ratios of WIBC to total BC (WIBC + WSBC) (hereafter referred to as the WIBC ratio) at the surface and the 0.5 sigma level for the annual averages are shown in Fig. 7. The WIBC ratios at the surface calculated by the AGV method reach up to 50 % over the United States and Europe and up to 70 % over Asia, whereas they decrease along the outflow and reach values near zero over the remote ocean. At the 0.5 sigma level, the WIBC ratio ranges from 10 to 40 % and up to 60 % near biomass burning regions. Compared with the WIBC ratio calculated by the AGF method, the ratio calculated

ACPD
12, 29801–29849, 2012

by the AGV method is larger by 10 % at the surface over most areas, by 50 % at the surface over the Arctic and by 30 % at the 0.5 sigma level. Therefore, the timescale of aging according to the AGV method (the new method in the present study) tends to be longer than that in the AGF method (the traditional method). This result leads to the difference in the simulated BC mass concentration near the source region shown in Fig. 4 and indicates that WIBC in the AGV method is less rapidly aged and thus less scavenged through wet deposition compared with that in the AGV method. In addition, the BC distribution over remote regions is determined by the efficiency of scavenging near both the limited BC source region and the outflow areas. Therefore, the difference in the simulated BC mass concentration over remote areas is remarkable, as shown in Fig. 4. Moreover, the distribution and ratios calculated by the AGV method are quite different from those calculated by the ORIG method. The WIBC ratios at the surface calculated by the ORIG method range from 10 to 30 % over the BC source regions (United States, Europe, China, and India) and become smaller over oceans, ranging from 30 to 40 %. At the 0.5 sigma level, the WIBC values exceed 90 % in the ORIG method. Therefore, in the ORIG method, the tendency observed for the WIBC ratio from the BC source regions to the outflow regions and to the upper regions is completely opposite to that observed using the AGV method. Theoretically, the WIOC ratios over BC source regions (lands) tend to be higher than those over outflow regions (oceans) because BC particles are aged by gases and aerosols in proportion to the suspension time in the atmosphere. Actually, the observed ratios were estimated to be 37 to 65 % in the spring in Tokyo, as suggested by Moteki et al. (2007), and 60 % in the summer in Tokyo, as suggested by Shiraiwa et al. (2007). In the upper area, the observed ratios are 15 % over the East Asia Sea, as indicated by Clarke et al. (2004), and 60 % in July above the boundary layers over North America, as indicated by Schwarz et al. (2006); thus, the WIBC ratios calculated by the ORIG method are unrealistic compared with the results obtained by the AGV method. This result means that the hygroscopicity of BC in the original SPRINTARS model over remote areas and upper altitudes is inconsistent with the observed hygroscopicity. The WIBC ratios calculated by the AGV method are

ACPD
12, 29801–29849, 2012

the closest to the observational data among those calculated using all three methods in the present study. In summary, the results show that the difference in the WIBC ratio between the AGV and the other (AGF and ORIG) methods is extremely large, which leads to a difference in the BC distribution and affects the radiative forcing due to BC particles.

3.2 Aerosol radiative property

In this section, simulated aerosol optical properties (AOT and AAOT) are compared with observations in Figs. 8 to 10. Figure 8 illustrates comparisons of these optical properties using AERONET results retrieved from the NASA Team algorithm under clear-sky conditions (Holben et al., 1998). The simulated AOT values in all experiments conducted in the present study are almost comparable to the AERONET-AOT values, falling within 20 % of each other over most areas, except South Africa and South America (where the difference in AOT values between simulations and observations is approximately 50 %). Other global aerosol-transport models using the same emission inventory of biomass burning used in this study also underestimate the simulated AOT values (e.g. Chin et al., 2009), which suggests that the emission inventory of biomass burning estimated using a bottom-up approach can be underestimated, as indicated by Kaiser et al. (2012). Thus, the simulated AAOT values are underestimated compared with the retrieved AAOT values, with the difference ranging from 30 to 70 %. The global model ECHAM-HAM reported by Stier et al. (2007) also underestimated AAOT values. Compared with the AAOT results reported by Stier et al. (2007), the simulated AAOT values in the present study are larger, especially over Asia and remote areas. This result is most likely because the emission inventory of anthropogenic BC used in the present study is larger than that used in other studies to adjust the BC surface mass concentrations over India (Goto et al., 2011a). However, the simulated AAOT values in the present study are still underestimated compared with the AERONET results. AeroCom models underestimated AAOT values in a study by Koch et al. (2009). Therefore, BC emission inventories may still be underestimated or AERONET-AAOT may be

ACPD
12, 29801–29849, 2012

overestimated because AERONET-AAOT can be retrieved only under high-AOT conditions (Dubovik et al., 2002).

To further investigate the difference in aerosol optical properties among the the methods, Figs. 9 and 10 present the global distribution of annual mean AOT and AAOT values under all-sky conditions. Globally, the difference in the AOT values simulated by the AGV and AGF methods ranges from −5 to +5 % (Fig. 9b). In East Asia, for example, the AOT values range from 0.3 to 1; therefore, the difference in AOT value between the AGV and AGF methods is estimated to be at most 0.05. By contrast, the relative difference in AOT values between the AGV and ORIG methods over aerosol source regions, such as North America, Europe, and Southeast Asia, is calculated to be slightly positive, with values of up to 5 %, whereas the difference over other areas is largely negative, with values ranging from −20 to −5 % (Fig. 9c). For AAOT, the values simulated by the AGV method are larger than those simulated by the AGF method by up to 50 % (Fig. 10b). The differences in the AAOT values simulated by the AGV and ORIG methods range from −20 to 20 % (Fig. 10c).

Apparently, these relative differences in AAOT are strongly related to the relative differences in the BC column burden shown in Fig. 6. However, over some regions, such as China, the correspondences between AAOT and the BC column burden are weak because AAOT is determined not only by the BC column burden but also by the difference in both the ratio of WIBC to total BC and the absorption coefficient of BC-containing particles. Compared with the AAOT results, the AOT results are more difficult because the difference in the extinction coefficients of BC-containing particles among the experiments is small, as shown in Fig. 1 and suggested by Oshima et al. (2009b). As shown in Fig. 12b from Goto et al. (2011a), the distribution of positive values in Fig. 10b corresponds to the distribution of the sulfate burden. In terms of sulfate, the AGV method considers two types of sulfate (sulfate that is externally and internally mixed with BC) with sizes of 69.5 and 100 nm, respectively, whereas the AGF method considers only externally mixed sulfate with a size of 69.5 nm. In the present study, we assumed that the hygroscopicities of both types of sulfate are the same,

ACPD
12, 29801–29849, 2012

such that internally mixed sulfate with a size of 100 nm is more easily scavenged from the atmosphere. As a result, the AOT of sulfate in the AGV method could be smaller than that of sulfate in the AGF method, although the extinction coefficients of sulfate internally mixed with BC are larger than those of externally mixed sulfate (see Sect. 2). In contrast, the difference in AOT between the AGV and ORIG methods is a result of the variation in the sulfate and BC column burden, the fraction of WSBC to total BC, and the extinction coefficients with hygroscopicity, as shown in Fig. 1.

4 Discussion of BC radiative forcing

In this section, we only discuss BC-ARF because we include neither cryosphere forcing caused by the deposition of BC onto snow and ice surfaces nor indirect aerosol forcing caused by BC particles acting as ice nuclei. The estimated BC-ARF values are presented in Table 3. At the tropopause, the annual and global mean BC-ARF values under all-sky conditions are estimated to be +0.30 (AGV), +0.05 (AGF), and +0.36 Wm^{-2} (ORIG). These results are close to or slightly smaller than the range (from +0.23 to +0.33 Wm^{-2} for only anthropogenic BC-ARF and from +0.33 to +0.47 Wm^{-2} for both anthropogenic and natural BC-ARF) derived from recent model estimates (Bauer et al., 2007; Unger et al., 2009; Myhre et al., 2009; Koch et al., 2011; Bond et al., 2011). At the surface, the forcing values due to total BC are estimated to be −0.87 Wm^{-2} (AGV), −0.42 Wm^{-2} (AGF), and −0.82 Wm^{-2} (ORIG), whereas those due to anthropogenic BC were estimated to be −0.49 Wm^{-2} by Koch et al. (2011). This result means that the values of atmospheric heating reported by Koch et al. (2011) are within the range estimated in the present study. Therefore, the difference in BC-ARF at the tropopause between the present study and previous studies could be caused by a difference in BC optical properties and the stratification of cloud layers and air mass containing BC compounds. The former reason is supported by the difference in the strength of absorption for pure BC, as discussed in Sect. 2. The latter reason is also supported by the studies of Haywood and Shine (1995) and Samset and Myhre (2009).

ACPD
12, 29801–29849, 2012

The largest differences in the ARF among the simulations in the present study are 0.31 Wm^{-2} (tropopause) and 0.45 Wm^{-2} (surface). The difference at the tropopause is comparable to the uncertainty estimated by AeroCom (Schulz et al., 2006) and IPCC-AR4 (Forster et al., 2007) studies. Therefore, we find that the BC-ARF values are highly influenced by the treatment of aging processes in the model and that the traditional method (AGF) leads to the underestimation of BC radiative forcings because the compounds mixed with BC are ignored.

To further investigate the impact of the different methods on BC-ARF at regional scales, Fig. 11 shows scatter plots of (a) the amount of BC emission and the BC column burden, as well as differences in (b) AOT, (c) AAOT, (d) BC-ARF at the tropopause, and (e) BC-ARF at the surface between the three (AGV, AGF and ORIG) methods with/without the use of regional BC aerosol averages. As the amount of BC emissions increases, not only the magnitudes of the parameters in Fig. 11 but also those of the differences among the three simulations increase. The largest differences in each parameter among the simulations are found over the South and East Asia regions. The differences in BC column burden, AOT, and AAOT were discussed in the previous paragraph; thus, here we discuss the regional BC-ARF values both at the surface and at the tropopause. In Fig. 11d and e, the BC-ARF values obtained by the AGV method lie between those obtained by the AGF and ORIG methods. Thus, the difference in the BC-ARF values obtained by the AGF and ORIG methods is estimated to be up to approximately 2 Wm^{-2} at the tropopause and approximately 3 Wm^{-2} at the surface over East Asia. Therefore, possible differences in the treatments of the BC aging process among global aerosol transport models produce large differences in BC-ARF values, especially over large BC emission areas such as South and East Asia.

Finally, we investigate the correlations between two different normalized efficiencies: (1) forcing efficiency (β_n), defined as the ratio of BC-ARF to the difference in AOT between experiments with/without BC aerosols, BC-ARF/ΔAOT; and (2) BC specific forcing efficiency (β_s), defined as the ratio of BC-ARF to the difference in the BC column burden between experiments with/without BC aerosols, BC-ARF/ΔBC, at the

ACPD
12, 29801–29849, 2012

tropopause and surface as a regional average. β_n is useful for properly evaluating the impacts of the total aerosol amount on the ARF under the various AOT conditions considered (e.g. Nakajima et al., 2007). β_s is also useful in understanding the impacts of specific aerosol compounds on the ARF under conditions corresponding to various amounts of BC. At the same time, β_s can be a helpful indicator for use in the creation of policies to control the concentration of specific aerosols to preserve air quality and address climate change. The correlations between β_n and β_s are shown in Fig. 12. As shown in Fig. 12a, at the tropopause, the values of β_n and β_s determined by the AGV method are larger than those determined by the AGF method, whereas the ranges of both parameters obtained by the AGV method are similar to those obtained by the ORIG method, even though there are large differences in each region. The fact that the AGV and ORIG methods take into account attached compounds (OC or sulfate) greatly affects the calculated radiative efficiency, indeed to a greater extent than that estimated in the AGF method, which ignores attached compounds in WSBC particles. The AGV method, which takes into account BC-sulfate mixed particles, produces large values of β_n and β_s in industrial areas (North America and Europe), whereas the ORIG method, which addresses BC-OC mixed particles, produces large values of β_n and β_s over biomass burning areas (South America and Central Africa). In Asia, including both biomass burning and industrial regions, the radiative impact of BC-OC was observed to be larger than that of BC-sulfate in the present study. The large values of β_n and β_s over biomass burning areas are also caused by the stratification of absorbing aerosols and low-level clouds, which enhance the absorption of aerosols and thereby produce larger positive radiative forcing than that observed under typical conditions (e.g. Haywood and Shine, 1997; Oikawa et al., 2012).

Figure 12b shows the values of β_n and β_s at the surface according to the three (AGV, AGF, and ORIG) methods. In addition to those at the tropopause shown in Fig. 12a, the efficiencies obtained by the AGV method become large in industrial regions, such as Europe and North America, mainly because the amounts of sulfate precursor, SO_2, emitted are large and partly because the amounts of BC emitted are much lower than

ACPD
12, 29801–29849, 2012

those in the biomass burning areas and other industrial regions, including developing countries. In reality, sulfates are often internally mixed with BC over Europe and North America, as indicated by Aerodyne aerosol mass spectrometer (AMS) measurements (e.g. Alfarra et al., 2004; McMeeking et al., 2010); therefore, global climate models that do not account for BC particles internally mixed with sulfate compounds may yield large errors regarding the effects of BC emission on the radiative impact at the surface. Therefore, it should be noted that the way in which mixtures of BC and other compounds are accounted for has a significant impact on the normalized ARF both at the tropopause and at the surface, depending on whether regions are controlled by biomass burning and/or by industrial areas.

5 Conclusions

To understand the effect of aging processes and the mixing state of black carbon (BC) on the spatial distribution of BC and aerosol direct radiative forcing due to BC compounds (BC-ARF), in the present study, we used three different methods of incorporating BC aging processes into a global aerosol transport model, SPRINTARS: (1) the AGV method, using a variable conversion rate τ_{BC} calculated by a new type of parameterization depending on both BC amount and sulfuric acid (Oshima and Koike, 2012); (2) the AGF method, which is widely used in other GCMs; and (3) the ORIG method, which is used in the original version of SPRINTARS. Over industrial regions, the differences in the surface BC mass concentration between simulations and observations are larger than those among the three methods; therefore, the aging process of BC particles in the model is less important in determining the mass concentration of BC over BC source regions than the BC emissions inventory. Moreover, the calculated hygroscopicities of BC particles were very different among the numerical simulations conducted using the three different BC aging methods. Near BC source regions, for example, the ratios of the amount of simulated water-insoluble BC (WIBC) to the total amount of BC (WIBC ratio) were estimated to be 80–90 % (AGV), 80–90 % (AGV) and

ACPD
12, 29801–29849, 2012

50–60 % (ORIG). These differences led to differences in the aerosol optical thickness (AOT) and absorption AOT calculated from the numerical simulations; as a result, the difference in the BC-ARF values calculated by the various treatments of the BC aging process was estimated to be at most 0.3 Wm^{-2}, which is comparable to the uncertainty suggested by IPCC-AR4 (2007) and the AeroCom results of Schulz et al. (2006).

Furthermore, we estimated the forcing efficiency normalized aerosol optical thickness (BC-ARF/ΔAOT) and specific forcing efficiency normalized by the BC burden (BC-ARF/ΔBC). We found that the values of BC-ARF/ΔAOT and BC-ARF/ΔBC at the surface calculated using the methods that take into account compounds attached to WSBC particles (i.e. AGV and ORIG) are quite different among different regions; the AGV method in particular shows large variability among the regions, including Europe and the United States. However, the values obtained using the method that does not take into account compounds attached to WSBC particles (i.e. the AGF method) do not vary with region. Therefore, the normalized forcing efficiencies obtained by the AGF method, which is widely used in most global climate models, could be underestimated. These differences in the calculated efficiency may be important with regard to the creation of political policies associated with CO_2 and BC emissions to address the issue of climate change.

Acknowledgements. Some of the authors were supported by projects from the Global Environment Research Fund B-0803 and A-1101 of the Ministry of Environment in Japan, the SALSA project of the Research Program on Climate Change Adaptation in Ministry of Education and Sports in Japan, and JSPS KAKENHI (Grant Number 24110002 and 23710029). The model simulations were performed using the supercomputer system NEC SX-8R/128M16 at the National Institute for Environmental Studies, Japan. We acknowledge the PIs and their staff for providing the IMPROVE, EMEP, and AERONET data, researchers for providing the NCAR/NCEP reanalysis data and HadISST data, and developers of the MIROC and SPRINTARS models. We also thank M. Koike and H. Matsui for their helpful discussions.

ACPD
12, 29801–29849, 2012

References

Adachi, K. and Buseck, P. R.: Internally mixed soot, sulfates, and organic matter in aerosol particles from Mexico City, Atmos. Chem. Phys., 8, 6469–6481, doi:10.5194/acp-8-6469-2008, 2008.

Alfarra, M. R., Coe, H., Allan, J. D., Bower, K. N., Boudries, H., Canagaratna, M. R., Jimenez, J. L., Jayne, J. T., Garforth, A. A., Li, S.-M., and Worsnop, D. R.: Characterization of urban and rural organic particulate in the Lower Fraser Valley using two Aerodyne Aerosol Mass Spectrometers, Atmos. Environ., 38, 5745–5758, 2004.

Bauer, S. E., Wright, D. L., Koch, D., Lewis, E. R., McGraw, R., Chang, L.-S., Schwartz, S. E., and Ruedy, R.: MATRIX (Multiconfiguration Aerosol TRacker of mIXing state): an aerosol microphysical module for global atmospheric models, Atmos. Chem. Phys., 8, 6003–6035, doi:10.5194/acp-8-6003-2008, 2008.

Bellouin, N., Boucher, O., Haywood, J., Johnson, C., Jones, A., Rae, J., and Woodward, S.: Improved representation of aerosols for HadGEM2, Hadley Centre technical note 73, Met Office, Exeter, UK, 43 pp., 2007.

Bodhaine, B. A.: Aerosol absorption measurements at Barrow, Mauna Loa and the south pole, J. Geophys. Res., 100, 8967–8975, 1995.

Bond, T. C. and Bergstrom, R. W.: Light absorption by carbonaceous particles: an investigative review, Aerosol Sci. Tech., 40, 27–67, 2006.

Bond, T. C., Bhardwaj, E., Dong, R., Jogani, R., Jung, S., Roden, C., Streets, D. G., and Trautmann, N. M.: Historical emissions of black and organic carbon aerosol from energy-related combustion, 1850–2000, Global Biogeochem. Cycle, 21, GB2018, doi:10.1029/2006GB002840, 2007.

Bond, T. C., Zarzycki, C., Flanner, M. G., and Koch, D. M.: Quantifying immediate radiative forcing by black carbon and organic matter with the Specific Forcing Pulse, Atmos. Chem. Phys., 11, 1505–1525, doi:10.5194/acp-11-1505-2011, 2011.

Chin, M., Ginoux, P., Kinne, S., Torres, O., Holben, B. N., Duncan, B. N., Martin, R. V., Logan, J. A., Higurashi, A., and Nakajima, T.: Tropospheric aerosol optical thickness from the GOCART model and comparisons with satellite and sun photometer measurements, J. Atmos. Sci., 59, 461–483, 2002.

ACPD
12, 29801–29849, 2012

Chin, M., Diehl, T., Dubovik, O., Eck, T. F., Holben, B. N., Sinyuk, A., and Streets, D. G.: Light absorption by pollution, dust, and biomass burngin aerosols: a global model study and evaluation with AERONET measurements, Ann. Geophys.-Germany, 27, 3439–3464, 2009.

Chung, S. H. and Seinfeld, J. H.: Global distribution and climate forcing of carbonaceous aerosols, J. Geophys. Res., 107, 4407, doi:10.1029/2001JD001397, 2002.

Clarke, A. D., Shinozuka, Y., Kapustin, V. N., Howell, S., Huebert, B., Doherty, S., Anderson, T., Covert, D., Anderson, J., Hua, X., Moore II, K. G., McNaughton, C., Carmichael, G., and Weber, R.: Size distributions and mixtures of dust and black carbon aerosol in Asian outflow: Physiochemistry and optical properties, J. Geophys. Res., 109, D15S09, doi:10.1029/2003JD004378, 2004.

Cooke, W. F. and Wilson, J. J. N.: A global black carbon aerosol model, J. Geophys. Res., 101, 19395–19409, 1996.

Croft, B., Lohmann, U., and von Salzen, K.: Black carbon ageing in the Canadian Centre for Climate modelling and analysis atmospheric general circulation model, Atmos. Chem. Phys., 5, 1931–1949, doi:10.5194/acp-5-1931-2005, 2005.

Davies, D. K., Ilavajhala, S., Wong, M. M., and Justice, C. O.: Fire Information for Resource Management System: Archiving and Distributing MODIS Active Fire Data, IEEE T. Geosci. Remote, 47, 72–79, doi:10.1109/TGRS.2008.2002076, 2009.

Dubovik, O., Holben, B., Eck, T. F., Smirnov, A., Kaufman, Y. J., King, M. D., Tanré, D., and Slutsker, I.: Variability of absorption and optical properties of key aerosol types observed in worldwide locations, J. Atmos. Sci., 59, 590–608, 2002.

Easter, R. C., Ghan, S. J., Zhang, Y., Saylor, R. D., Chapman, E. G., Laulainen, N. S., Abdul-Razzak, H., Lenug, L. R., Bian, X., and Zaveri, R. A.: MIRAGE: Model description and evaluation of aerosols and trace gases, J. Geophys. Res., 109, D20210, doi:10.1029/2004JD004571, 2004.

Eleftheriadis, K., Vratolis, S., and Nyeki, S.: Aerosol black carbon in the European Arctic: Measurements at Zeppelin station, Ny-Ålesund, Svalbard from 1998–2007, Geophys. Res., Lett., 36, L02809, doi:10.1029/2008GL035741, 2009.

Fast, J. D., Gustafson, Jr. W. I., Easter, R. C., Zaveri, R. A., Barnard, J. C., Chapman, E. G., Grell, G. A., and Peckham, S. E.: Evolution of ozone, particulates, and aerosol direct radiative forcing in the vicinity of Houston using a fully coupled meteorology-chemistry-aerosol model, J. Geophys. Res., 111, D21305, doi:10.1029/2005JD006721, 2006.

ACPD
12, 29801–29849, 2012

Flanner, M. G., Zender, C. S., Hess, P. G., Mahowald, N. M., Painter, T. H., Ramanathan, V., and Rasch, P. J.: Springtime warming and reduced snow cover from carbonaceous particles, Atmos. Chem. Phys., 9, 2481–2497, doi:10.5194/acp-9-2481-2009, 2009.

Forster, P., Ramaswamy, V., Artaxo, P., Berntsen, T., Betts, R., Fahey, D. W., Haywood, J., Lean, J., Lowe, D. C., Myhre, G., Nganga, J., Prinn, R., Raga, G., Schulz, M., and Van Dorland, R.: Changes in Atmospheric Constituents and in Radiative Forcing, in: Climate Change 2007: The Physical Science Basis, Contribution of Working Group I to the Fourth Assessment Report of the Intergovernmental Panel on Climate Change, edited by: Solomon, S., Qin, D., Manning, M., Chen, Z., Marquis, M., Averyt, K. B., Tignor, M., and Miller, H. L., Cambridge University Press, Cambridge, United Kingdom and New York, NY, USA, 996 pp., 2007.

Goto, D., Takemura, T., and Nakajima, T.: Importance of global aerosol modeling including secondary organic aerosol formed from monoterpene, J. Geophys. Res., 113, D07205, doi:10.1029/2007JD009019, 2008.

Goto, D., Nakajima, T., Takemura, T., and Sudo, K.: A study of uncertainties in the sulfate distribution and its radiative forcing associated with sulfur chemistry in a global aerosol model, Atmos. Chem. Phys., 11, 10889–10910, doi:10.5194/acp-11-10889-2011, 2011a.

Goto, D., Schutgens, N. A. J., Nakajima, T., and Takemura, T.: Sensitivity of aerosol to assumed optical properties over Asia using a global aerosol model and AERONET, Geophys. Res. Lett., 38, L17810, doi:10.1029/2001GL048675, 2011b.

Goto, D., Takemura, T., Nakajima, T., and Badarinath, K. V. S.: Global aerosol model-derived black carbon concentration and single scattering albedo over Indian region and its comparison with ground observations, Atmos. Environ., 45, 3277–3285, 2011c.

Guazzotti, S. A., Coffee, K. R., and Prather, K. A.: Continuous measurements of size-resolved particle chemistry during INDOEX-Intensive Field Phase 99, J. Geophys. Res., 106, 28607–28627, 2001.

Hansen, J., Sato, M., and Ruedy, R.: Radiative forcing and climate response, J. Geophys. Res., 102, 6831–6864, 1997.

Haywood, J. M. and Shine, K. P.: Multi-spectral calculations of the direct radiative forcing of tropospheric sulphate and soot aerosols using a column model, Q. J. Roy. Meteor. Soc., 123, 1907–1930, 1997.

Hess, M., Koepke, P., and Schult, I.: Optical Properties of Aerosols and Clouds: The Software Package OPAC, B. Am. Meteo. Soc., 79, 831–844, 1998.

ACPD
12, 29801–29849, 2012

Holben, B., Eck, T. F., Slutsker, I., Tanré, D., Buis, J. P., Setzer, A., Vermore, E., Reagan, J. A., Kaufman, Y. J., Nakajima, T., Lavenu, F., Jankowiak, I., and Smirnov, A.: AERONET-A Federated Instrument Network and Data Archive for Aerosol Characterization, Remote Sens. Environ., 66, 1–16, 1998.

Jacobson, M. Z.: Strong radiative heating due to the mixing state of black carbon in atmospheric aerosols, Nature, 409, 695–697, 2001.

Jacobson, M. Z.: Control of fossil-fuel particulate black carbon and organic matter possibly the most effective method of slowing global warming, J. Geophys. Res., 107, 4410, doi:10.1029/2001JD001376, 2002.

Jacobson, M. Z.: Development of mixed-phase clouds from multiple aerosol size distributions and the effect of the clouds on aerosol removal, J. Geophys. Res., 108, 4245, doi:10.1029/2002JD002691, 2003.

Johnson, K. S., Zuberi, B., Molina, L. T., Molina, M. J., Iedema, M. J., Cowin, J. P., Gaspar, D. J., Wang, C., and Laskin, A.: Processing of soot in an urban environment: case study from the Mexico City Metropolitan Area, Atmos. Chem. Phys., 5, 3033–3043, doi:10.5194/acp-5-3033-2005, 2005.

K-1 Model Developers: K-1 coupled GCM (MIROC) description, K-1 Tech. Rep. 1, edited by: Hasumi, H. and Emori, S., Univ. of Tokyo, Tokyo, 34 pp., 2004.

Katrinak, K. A., Rez, P., and Buseck, P. R.: Structural variations in individual carbonaceous particles from an urban aerosol, Environ. Sci. Technol., 26, 1967–1976, 1992.

Kim, Y. J., Kim, M. J., Lee, K. H., and Park, S. S.: Investigation of carbon pollution episodes using semi-continuous instrument in Incheon, Korea, Atmos. Environ., 40, 4054–4075, 2006.

Kim, H. S., Huh, J. B., Hopke, P. K., Holsen, T. M., Yi, S. M.: Characteristics of the major chemical constituents of $PM_{2.5}$ and smog events in Seoul, Korea in 2003 and 2004, Atmos. Environ., 41, 6762–6770, 2007.

Kim, D. C., Wang, C., Ekman, A. M. L., Barth, M. C., and Rasch, P. J.: Distribution and direct radiative forcing of carbonaceous and sulfate aerosols in an interactive size-resolving aerosol-climate model, J. Geophys. Res., 113, D16309, doi:10.1029/ 2007JD009756, 2008.

Koch, D. and Hansen, J.: Distant origins of Arctic black carbon: A Goddard Institute for Space Studies ModelE experiment, J. Geophys. Res., 110, D42024, doi:10.1029/2004JD005296, 2005.

Koch, D., Schulz, M., Kinne, S., McNaughton, C., Spackman, J. R., Balkanski, Y., Bauer, S., Berntsen, T., Bond, T. C., Boucher, O., Chin, M., Clarke, A., De Luca, N., Dentener, F., Diehl,

ACPD
12, 29801–29849, 2012

T., Dubovik, O., Easter, R., Fahey, D. W., Feichter, J., Fillmore, D., Freitag, S., Ghan, S., Ginoux, P., Gong, S., Horowitz, L., Iversen, T., Kirkevåg, A., Klimont, Z., Kondo, Y., Krol, M., Liu, X., Miller, R., Montanaro, V., Moteki, N., Myhre, G., Penner, J. E., Perlwitz, J., Pitari, G., Reddy, S., Sahu, L., Sakamoto, H., Schuster, G., Schwarz, J. P., Seland, Ø., Stier, P., Takegawa, N., Takemura, T., Textor, C., van Aardenne, J. A., and Zhao, Y.: Evaluation of black carbon estimations in global aerosol models, Atmos. Chem. Phys., 9, 9001–9026, doi:10.5194/acp-9-9001-2009, 2009.

Koch, D., Bauer, S. E., Del Genio, A., Faluvegi, G., McConnell, J. R., Menon, S., Miller, R. L., Rind, D., Ruedy, R., Schmidt, G. A., and Shindell, D.: Coupled aerosol-chemistry-climate twentieth-century transient model investigation: trends in short-lived species and climate responses, J. Climate, 24, 2693–2714, 2011.

Kondo, Y., Komazaki, Y., Miyazaki, Y., Moteki, N., Takegawa, N., Kodama, D., Deguchi, S., Nogami, M., Fukuda, M., Miyakawa, T., Morino, Y., Koike, M., Sakurai, H., and Ehara, K.: Temporal variations of elemental carbon in Tokyo, J. Geophys. Res., 111, D12205, doi:10.1029/2005JD006257, 2006.

Kozlov, V. S., Panchenko, M. V., and Yausheva, E. P.: Mass fraction of black carbon in submicron aerosols as an indicator of influence of smoke from remote forest fires in Siberia, Atmos. Environ., 42, 2611–2620, 2006.

Liao, H., Seinfeld, J. H., Adams, P. J., and Mickley, L. J.: Global radiative forcing of coupled tropospheric ozone and aerosols in a unified general circulation model, J. Geophys. Res., 109, D16207, doi:10.1029/2003JD004456, 2004.

Liu, X. H., Penner, J. E., and Herzog, M.: Global modeling of aerosol dynamics: Model description, evaluation, and interactions between sulfate and nonsulfate aerosols, J. Geophys. Res., 110, D18026, doi:10.1029/2004JD005674, 2005.

Liu, J. F., Fan, S. M., Horoqitz, L. W., and Levy II, H.: Evaluation of factors controlling long-range transport of black carbon to the Arctic, J. Geophys. Res., 116, D04307, doi:10.1029/2010JD015145, 2011.

Matsumoto, K., Minami, H., Hayano, T., Uyama, Y., Tanimoto, H., and Uematsu, M.: Regional climatology of particulate carbonaceous substances in the northern area of the east Asian Pacific rim, J. Geophys. Res., 112, D24203, doi:10.1029/2007JD008607, 2007.

McMeeking, G. R., Hamburger, T., Liu, D., Flynn, M., Morgan, W. T., Northway, M., Highwood, E. J., Krejci, R., Allan, J. D., Minikin, A., and Coe, H.: Black carbon measurements in the

ACPD
12, 29801–29849, 2012

boundary layer over western and northern Europe, Atmos. Chem. Phys., 10, 9393–9414, doi:10.5194/acp-10-9393-2010, 2010.
Menon, S., Hansen, J., Nazarenko, L., and Luo, Y. F.: Climate effects of black carbon aerosols in China and India, science, 297, 2250–2253, 2002.
Minoura, H., Takahashi, K., Chow, J. C., and Watson, J. G.: Multi-year trend in fine and coarse particle mass, carbon, and ions in downtown Tokyo, Japan, Atmos. Environ., 40, 2478–2487, 2006.
Moffet, R. C. and Prather, K. A.: In situ measurements of the mixing state and optical properties of soot: Implications for radiative forcing estimates, Proc. Natl. Acad, Sci. USA, 106, 11872–11877, 2009.
Moteki, N., Kondo, Y., Miyazaki, Y., Takegawa, N., Komazaki, Y., Kurata, G., Shirai, T., Blake, D. R., Miyakawa, T., and Koike, M.: Evolution of mixing state of black carbon particles: Aircraft measurements over the western Pacific in March 2004, Geophys. Res. Lett., 34, L11803, doi:10.1029/2006GL028943, 2007.
Myhre, G., Berglen, T. F., Johnsrud, M., Hoyle, C. R., Berntsen, T. K., Christopher, S. A., Fahey, D. W., Isaksen, I. S. A., Jones, T. A., Kahn, R. A., Loeb, N., Quinn, P., Remer, L., Schwarz, J. P., and Yttri, K. E.: Modelled radiative forcing of the direct aerosol effect with multi-observation evaluation, Atmos. Chem. Phys., 9, 1365–1392, doi:10.5194/acp-9-1365-2009, 2009.
Nakajima, T., Tsukamoto, M., Tsushima, Y., Numaguti, A., and Kimura, T.: Modeling of the radiative process in an atmospheric general circulation model, Appl. Opt., 39, 4869–4878, 2000.
Nakajima T., Yoon, S.-C., Ramanathan, V., Shi, G.-Y., Takemura, T., Higurashi, A., Takamura, T., Aoki, K., Sohn, B.-J., Kim, S.-W., Tsuruta, H., Sugimoto, N., Shimizu, A., Tanimoto, H., Sawa, Y., Lin, N.-H., Lee, C.-T., Goto, D., and Schutgens, N.: Overview of the Atmospheric Brown Cloud East Asian Regional Experiment 2005 and a study of the aerosol direct radiative forcing in east Asia, J. Geophys. Res., 112, D24S91, doi:10.1029/2007JD009009, 2007.
Naoe, H. and Okada, K.: Mixing properties of submicrometer aerosol particles in the urban atmosphere – with regard to soot particles, Atmos. Environ., 35, 5765–5772, 2001.
Oikawa, E., Nakajima, T., Inoue, T., and Winker, D.: A study of the shortwave direct aerosol forcing using ESSP/CALIPSO observation and GCM simulation, J. Geophys. Res., in review, 2012.
Okada, K.: Number-size distribution and formation process of submicrometer sulfate-containing particles in the urban atmosphere of Nagoya (Japan), Atmos. Environ., 19, 743–758, 1985.

ACPD
12, 29801–29849, 2012

Omar, A. H., Won, J.-G., Winker, D. M., Yoon, S.-C., Dubovik, O., and McConnick, M. P.: Development of global aerosol models using cluster analysis of Aerosol Robotic Network (AERONET) measurement, J. Geophys. Res., 110, D10S14, doi:10.1029/2004JD004874, 2005.

Oshima, N. and Koike, M.: Development of a parameterization of black carbon aging for use in general circulation models, Geosci. Model Dev. Discuss., 5, 1263–1293, doi:10.5194/gmdd-5-1263-2012, 2012.

Oshima, N., Koike, M., Zhang, Y., Kondo, Y., Moteki, N., Takegawa, N., and Miyazaki, Y.: Aging of black carbon in outflow from anthropogenic sources using a mixing state resolved model: Model development and evaluation, J. Geophys. Res., 114, D06210, doi:10.1029/2008JD010680, 2009a.

Oshima, N., Koike, M., Zhang, Y., and Kondo, Y.: Aging of black carbon in outflow from anthropogenic sources using a mixing state resolved model: 2. Aerosol optical properties and cloud condensation nuclei activities, J. Geophys. Res., 114, D18202, doi:10.1029/2008JD011681, 2009b.

Oshima, N., Kondo, Y., Moteki, N., Takegawa, N., Koike, M., Kita, K., Matsui, H., Kajino, M., Nakamura, H., Jung, J. S., and Kim, Y. J.: Wet removal of black carbon in Asian outflow: Aerosol Radiative Forcing in East Asia (A-FORCE) aircraft campaign, J. Geophys. Res., 117, D03204, doi:10.1029/2011JD016552, 2012.

Park, R., Jacob, D. J., Chin, M., and Martin, R. V.: Sources of carbonaceous aerosols over the United States and implications for natural visibility, J. Geophys. Res., 108, 4355, doi:10.1029/2002JD003190, 2003.

Parungo, F. Nagatomo, C., Zhou, M. Y., Hansen, A. D. A., and Harris, J: Aeolian transport of aerosol black carbon from China to the ocean, Atmos. Environ., 28, 3251–3260, 1994.

Pierce, J. R., Chen, K., and Adams, P. J.: Contribution of primary carbonaceous aerosol to cloud condensation nuclei: processes and uncertainties evaluated with a global aerosol microphysics model, Atmos. Chem. Phys., 7, 5447–5466, doi:10.5194/acp-7-5447-2007, 2007

Pósfai, M. and Buseck, P. R.: Nature and climate effects of individual tropospheric aerosol particles, Annu. Rev. Earth Planet. Sci., 38, 17–43, 2010.

Pósfai, M., Anderson, J. R., and Buseck, P. R.: Soot and sulfate aerosol particles in the remote marine troposphere, J. Geophys. Res., 104, 21685–21693, 1999.

Pratt, K. A. and Prather, K. A.: Aircraft measurements of vertical profiles of aerosol mixing states, J. Geophys. Res., 115, D11305, doi:10.1029/2009JD013150, 2010.

ACPD
12, 29801–29849, 2012

Randerson, J. T., van der Werf, G. R., Giglio, L., Collatz, G. J., and Kasibhatla, P. S.: Global Fire Emissions Database, Version 2 (GFEDv2). Data set. Available on-line (http://daac.ornl.gov/) from Oak Ridge National Laboratory Distributed Active Archive Center, Oak Ridge, Tennessee, USA, doi:10.3334/ORNLDAAC/834, 2006.

Reddy, M. S. and Boucher, O.: A study of the global cycle of carbonaceous aerosols in the LMDZT general circulation model, J. Geophys. Res., 109, D14202, doi:10.1029/2003JD004048, 2004.

Riemer, N., Vogel, H., and Vogel, B.: Soot aging time scales in polluted regions during day and night, Atmos. Chem. Phys., 4, 1885–1893, doi:10.5194/acp-4-1885-2004, 2004.

Riemer, N., West, M., Zaveri, R. A., and Easter, R. C.: Simulating the evolution of soot mixing state with a particle-resolved aerosol model, J. Geophys, Res., 114, D09202, doi:10.1029/2008JD011073, 2009.

Schulz, M., Textor, C., Kinne, S., Balkanski, Y., Bauer, S., Berntsen, T., Berglen, T., Boucher, O., Dentener, F., Guibert, S., Isaksen, I. S. A., Iversen, T., Koch, D., Kirkevåg, A., Liu, X., Montanaro, V., Myhre, G., Penner, J. E., Pitari, G., Reddy, S., Seland, Ø., Stier, P., and Takemura, T.: Radiative forcing by aerosols as derived from the AeroCom present-day and pre-industrial simulations, Atmos. Chem. Phys., 6, 5225–5246, doi:10.5194/acp-6-5225-2006, 2006.

Schwarz, J. P., Gao, R. S., Fahey, D. W., Thomson, D. S., Watts, L. A., Wilson, J. C., Reeves, J. M., Darbeheshti, M., Baumgardner, D. G., Kok, G. L., Chung S. H., Schulz, M., Hendricks, J., Lauer, A., Kärcher, B., Slowik, J. G., Rosenlof, K. H., Thompson, T. L., Langford, A. O., Loewenstein, M., and Aikin, K. C.: Single-particle measurements of midlatitute black carbon and light-scattering aerosols from the boundary layer to the lower stratosphere, J Geophys. Res., 111, D16207, doi:10.1029/2006JD007076, 2006.

Schwarz, J. P., Spackman, J. R., Fahey, D. W., Gao, R. S., Lohmann, U., Stier, P., Watts, L. A., Thomson, D. S., Lack, D. A., Pfister, L., Mahoney, M. J., Baumgardner, D., Wilson, J. C., and Reeves, J. M.: Coatings and their enhancement of black carbon light absorption in the tropical atmosphere, J. Geophys. Res., 113, D03203, doi:10.1029/2007JD009042, 2008.

Seinfeld, J. H. and Pandis, S. N.: Atmospheric Chemistry and Physics: from air Pollution to Climate Change, John Wiley, New York, 1326 pp., 1998.

Sekiguchi, M. and Nakajima, T.: A k-distribution-based radiation code and its computational optimization for an atmospheric general circulation model. J. Quant. Spectrosc. Radiat. Transfer, 109, 2779–2793, 2008.

ACPD
12, 29801–29849, 2012

Sharma, S., Andrews, E., Barrie, L. A., Ogren, J. A., and Lavoué, D.: Variations and sources of the equivalent black carbon in the high Arctic revealed by long-term observations at Alert and Barrow: 1989–2003, J. Geophys. Res., 111, D14208, doi:10.1029/2005JD006581, 2006.

Shindell, D. T., Chin, M., Dentener, F., Doherty, R. M., Faluvegi, G., Fiore, A. M., Hess, P., Koch, D. M., MacKenzie, I. A., Sanderson, M. G., Schultz, M. G., Schulz, M., Stevenson, D. S., Teich, H., Textor, C., Wild, O., Bergmann, D. J., Bey, I., Bian, H., Cuvelier, C., Duncan, B. N., Folberth, G., Horowitz, L. W., Jonson, J., Kaminski, J. W., Marmer, E., Park, R., Pringle, K. J., Schroeder, S., Szopa, S., Takemura, T., Zeng, G., Keating, T. J., and Zuber, A.: A multi-model assessment of pollution transport to the Arctic, Atmos. Chem. Phys., 8, 5353–5372, doi:10.5194/acp-8-5353-2008, 2008.

Shiraiwa, M., Kondo, Y., Moteki, N., Takegawa, N., Miyazaki, Y., and Blake, D. R.: Evolution of mixing state of black carbon in polluted air from Tokyo, Geophys. Res. Lett., 34, L16803, doi:10.1029/2007GL029819, 2007.

Shiraiwa, M., Kondo, Y., Moteki, N., Takegawa, N., Sahu, L. K., Takami, A., Hatakeyama, S., Yonemura, S., and Blake, D. R.: Radiative impact of mixing state of black carbon aerosol in Asian outflow, J. Geophys. Res., 113, D24210, doi:10.1029/2008JD010546, 2008.

Stier, P., Feichter, J., Kinne, S., Kloster, S., Vignati, E., Wilson, J., Ganzeveld, L., Tegen, I., Werner, M., Balkanski, Y., Schulz, M., Boucher, O., Minikin, A., and Petzold, A.: The aerosol-climate model ECHAM5-HAM, Atmos. Chem. Phys., 5, 1125–1156, doi:10.5194/acp-5-1125-2005, 2005.

Stier, P., Seinfeld, J. H., Kinne, S., and Boucher, O.: Aerosol absorption and radiative forcing, Atmos. Chem. Phys., 7, 5237–5261, doi:10.5194/acp-7-5237-2007, 2007.

Streets, D. G., Bond, T. C., Carmichael, G. R., Fernandes, S. D., Fu, Q., He, D., Klimont, Z., Nelson, S. M., Tsai, N. Y., Wang, M. Q., Woo, J.-H., and Yarber, K. F.: An inventory of gaseous and primary aerosol emissions in Asia in the year 2000, J. Geophys. Res., 108, 8809, doi:10.1029/2002JD003093, 2003.

Suzuki, K., Nakajima, T., Numaguti, A., Takemura, T., Kawamoto, K., and Higurashi, A.: A study of the aerosol effect on a cloud field with simultaneous use of GCM modeling and satellite observation, J. Atmos. Sci., 61, 179–194, 2004.

Takahama, S., Liu, S., and Russell, L. M.: Coatings and clusters of carboxylic acids in carbon-containing atmospheric particles from spectromicroscopy and their implications for cloud-nucleating and optical properties, J. Geophys. Res., 115, D01202, doi:10.1029/2009JD012622, 2010.

ACPD
12, 29801–29849, 2012

Takemura, T., Okamoto, H., Maruyama, Y., Numaguti, A., Higurashi, A., and Nakajima, T.: Global three-dimensional simulation of aerosol optical thickness distribution of various origins, J. Geophys. Res., 105, 17853–17873, 2000.

Takemura, T., Nakajima, T., Dubovik, O., Holben, B. N., and Kinne, S.: Single scattering albedo and radiative forcing of various aerosol species with a global three-dimensional model, J. Climate, 15, 333–352, 2002.

Takemura, T., Nozawa, T., Emori, S., Nakajima, T. Y., and Nakajima, T.: Simulation of climate response to aerosol direct and indirect effects with aerosol transport-radiation model, J. Geophys. Res., 110, D02202, doi:10.1029/2004JD005029, 2005.

Takemura, T., Egashira, M., Matsuzawa, K., Ichijo, H., O'ishi, R., and Abe-Ouchi, A.: A simulation of the global distribution and radiative forcing of soil dust aerosols at the Last Glacial Maximum, Atmos. Chem. Phys., 9, 3061–3073, doi:10.5194/acp-9-3061-2009, 2009.

Textor, C., Schulz, M., Guibert, S., Kinne, S., Balkanski, Y., Bauer, S., Berntsen, T., Berglen, T., Boucher, O., Chin, M., Dentener, F., Diehl, T., Easter, R., Feichter, H., Fillmore, D., Ghan, S., Ginoux, P., Gong, S., Grini, A., Hendricks, J., Horowitz, L., Huang, P., Isaksen, I., Iversen, I., Kloster, S., Koch, D., Kirkevåg, A., Kristjansson, J. E., Krol, M., Lauer, A., Lamarque, J. F., Liu, X., Montanaro, V., Myhre, G., Penner, J., Pitari, G., Reddy, S., Seland, Ø., Stier, P., Takemura, T., and Tie, X.: Analysis and quantification of the diversities of aerosol life cycles within AeroCom, Atmos. Chem. Phys., 6, 1777–1813, doi:10.5194/acp-6-1777-2006, 2006.

Unger, N., Menon, S., Koch, D. M., and Shindell, D. T.: Impacts of aerosol-cloud interactions on past and future changes in tropospheric composition, Atmos. Chem. Phys., 9, 4115–4129, doi:10.5194/acp-9-4115-2009, 2009.

Vignati, E., Karl, M., Krol, M., Wilson, J., Stier, P., and Cavalli, F.: Sources of uncertainties in modelling black carbon at the global scale, Atmos. Chem. Phys., 10, 2595–2611, doi:10.5194/acp-10-2595-2010, 2010.

Watanabe, M., Suzuki, T., O'ishi, R., Komuro, Y., Watanabe, S., Emori, S., Takemura, T., Chikira, M., Ogura, T., Sekiguchi, M., Takata, K., Yamadaki, D., Tokohata, T., Nozawa, T., Hasumi, H., Tatebe, H., Kimoto, M: Improved climate simulation by MIROC 5: mean states, variability, and climate sensitivity, J. Climate, 23, 6312–6335, 2010.

Weingartner, E., Burtscher, H., and Baltensperger, U.: Hygroscopic properties of carbon and diesel soot particles, Atmos. Environ., 31, 2311–2327, 1997.

Wilson, J., Cuvelier, C., and Raes, F.: A modeling study of global mixed aerosol fields, J. Geophys. Res., 106, 34081–34108, 2001.

ACPD
12, 29801–29849, 2012

Wolff, E. W. and Cachier, H.: Concentrations and seasonal cycle of black carbon in aerosol at a coastal Antarctic station, J. Geophys. Res., 103, 11033–11041, 1995.

Zaveri, R. A., Easter, R. C., Fast, J. D., and Peters, L. K.: Model for Simulating Aerosol Interactions and Chemistry (MOSAIC), J. Geophys. Res., 113, D13204, doi:10.1029/2007JD008782, 2008.

Zhang, Y., Pun, B., Vijayaraghavan, K., Wu, S.-Y., Seigneur, C., Pandis, S. N., Jacobson, M. Z., Nenes, A., and Seinfeld, J. H.: Development and application of the Model of Aerosol Dynamics, Reaction, Ionization, and Dissolution (MADRID), J. Geophys. Res., 109, D01202, doi:10.1029/2003JD003501, 2004.

Zhang, X. Y., Wang, Y. Q., Zhang, X. C., Guo, W., and Gong, S. L.: Carbonaceous aerosol composition over various regions of China during 2006, J. Geophys. Res., 113, D14111, doi:10.1029/2007JD009525, 2008.

ACPD
12, 29801–29849, 2012

Table 1. Experimental designs employed in this study.

Method	Aging processes in the atmosphere		Internally mixed BC with other compounds		Reference
	Pure BC (WIBC)	Mixed BC (WSBC)	BC + OC	BC + SO_4	
AGV	Aged by variable decay time	Increase in aging	N	Y	This work
AGF	Aged by fixed decay time	Increase in aging	N	N	Chung and Seinfeld (2002)
ORIG	No aging	No increase in aging	Y	N	Takemura et al. (2005)

ACPD
12, 29801–29849, 2012

Table 2. Comparison of BC surface mass concentrations between the simulations and observations according to the annual averages (AVE), correlation coefficient (R), and normalized mean bias (NMB), where S_i represents the simulations for station i and O_i represents the observations made at station i.

Region		OBS	AGV	AGF	ORIG
US	AVE	0.20	0.74	0.74	0.76
	R		0.65	0.65	0.65
	NMB		1.22	1.22	1.31
Europe	AVE	0.81	0.29	0.29	0.31
	R		0.40	0.42	0.44
	NMB		−0.61	−0.61	−0.59
China	AVE	4.88	6.97	6.86	6.85
	R		0.47	0.46	0.46
	NMB		0.06	−0.03	0.06
India	AVE	3.10	3.82	3.78	3.83
	R		0.79	0.79	0.79
	NMB		−0.32	−0.33	−0.33
Other	AVE	6.02	6.32	6.25	6.31
	R		0.82	0.82	0.81
	NMB		−0.19	−0.2	−0.18

ACPD
12, 29801–29849, 2012

Table 3. Aerosol radiative forcing (ARF) due to the direct effect of the total BC obtained by the three different methods used in the present study under all-sky conditions.

	ARF value	
	Tropopause	Surface
AGV	+0.300	−0.870
AGF	+0.047	−0.424
ORIG	+0.356	−0.822
Chung and Seinfeld (2002)*	+0.51 to +0.8	
Unger et al. (2009)*	+0.313	
Myhre et al. (2009)*	+0.26 to +0.33	
Koch et al. (2011)*	+0.23	−0.49
Bauer et al. (2007)	+0.33	
Bond et al. (2011)	+0.47	

* ARF due to the direct effect of anthropogenic BC.

ACPD
12, 29801–29849, 2012

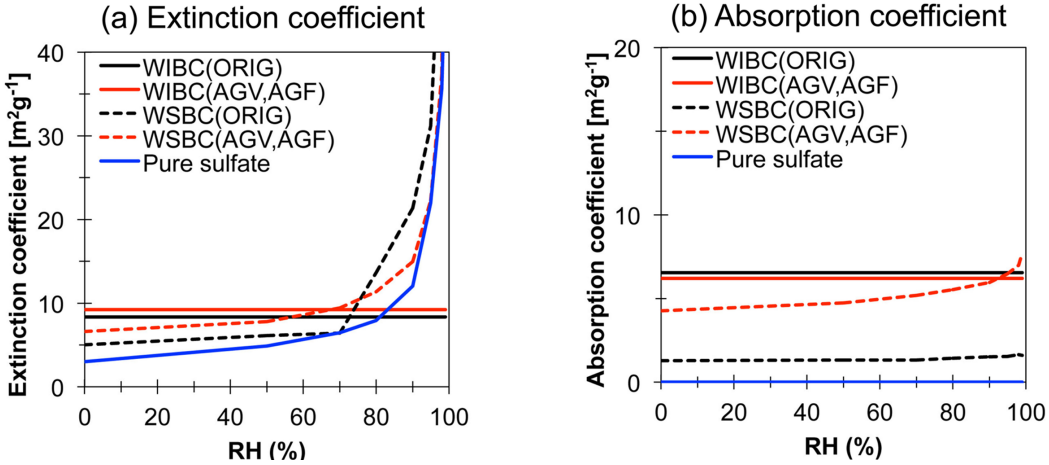

Fig. 1. Dependence of extinction and absorption coefficients for BC and sulfate particles on relative humidity (RH) in the present study.

ACPD
12, 29801–29849, 2012

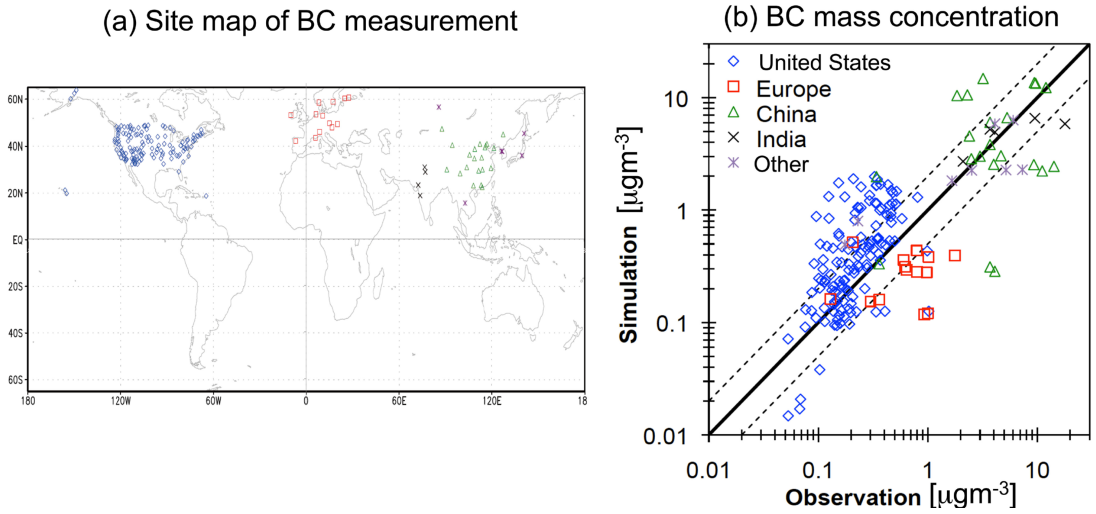

Fig. 2. Comparisons of simulated BC mass concentrations with observations. The observations are in the United States (IMPROVE), Europe (EMEP), China (Zhang et al., 2008), India (Goto et al., 2011c), and other Asian sites (Tokyo/Japan by Kondo et al., 2006 and Minoura et al., 2006; Rishiri/Japan by Matsumoto et al., 2007; Incheon/Korea by Kim et al., 2006; Seoul/Korea by Kim et al., 2007; Tomsk/Russia by Kozlov et al., 2008; Phimai/Thailand by H. Tsuruta, 2011, personal communication).

ACPD
12, 29801–29849, 2012

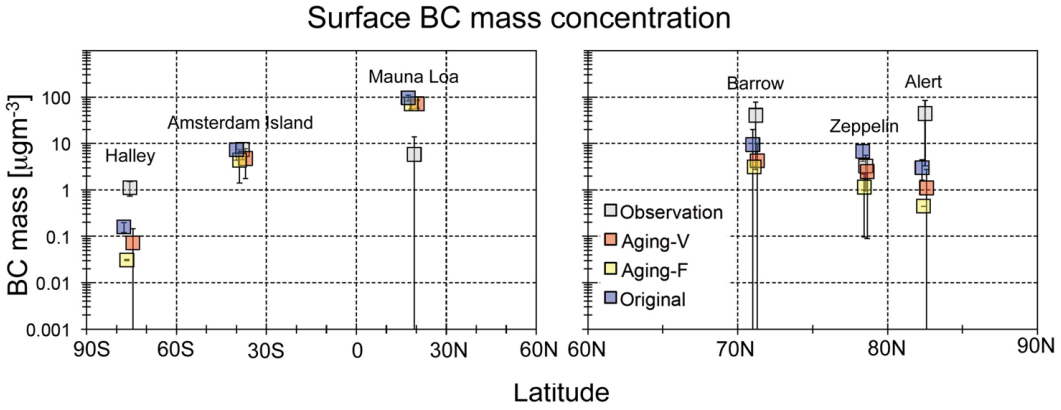

Fig. 3. Annually averaged BC mass concentrations at remote sites. The observations are in Amsterdam Island and Halley by Wolff and Cachier (1998), Alert and Barrow by Sharma et al. (2006), Zeppelin by Eleftheriadis et al. (2009), and Mauna Loa by Bodhaine (1995).

ACPD
12, 29801–29849, 2012

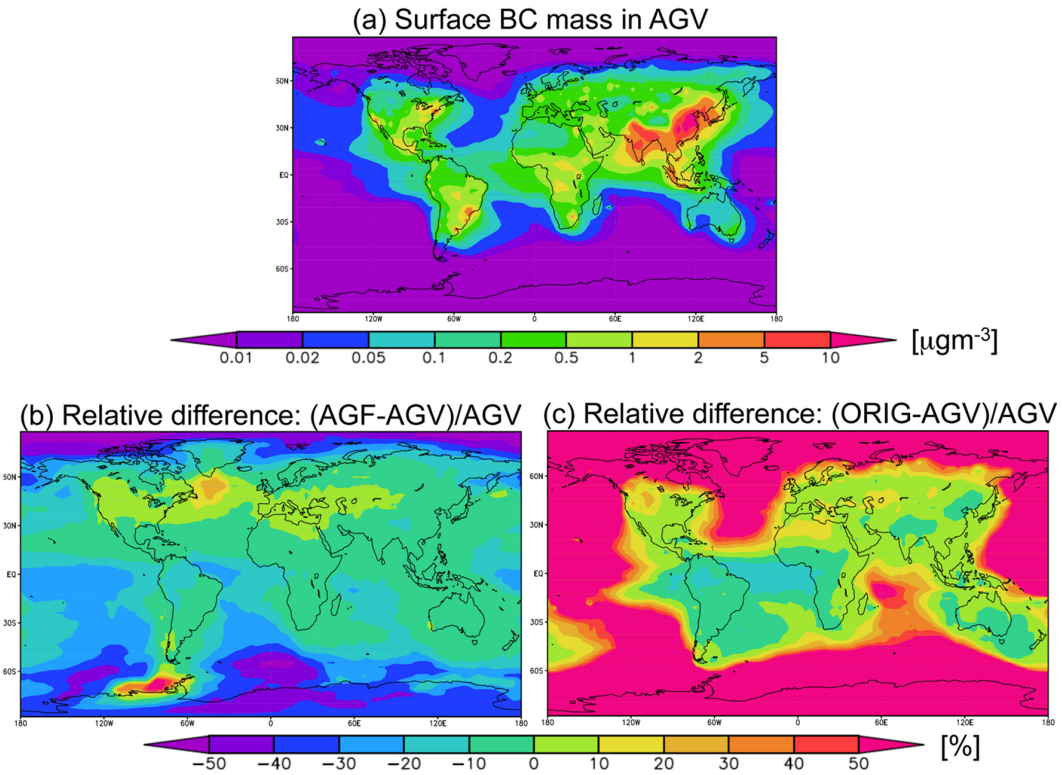

Fig. 4. A global map of annually averaged **(a)** surface BC mass concentration obtained by AGV method and relative difference in the BC mass concentration **(b)** between AGF and AGV and **(c)** between ORIG and AGV methods.

ACPD
12, 29801–29849, 2012

Radiative effect of different BC aging processes

D. Goto et al.

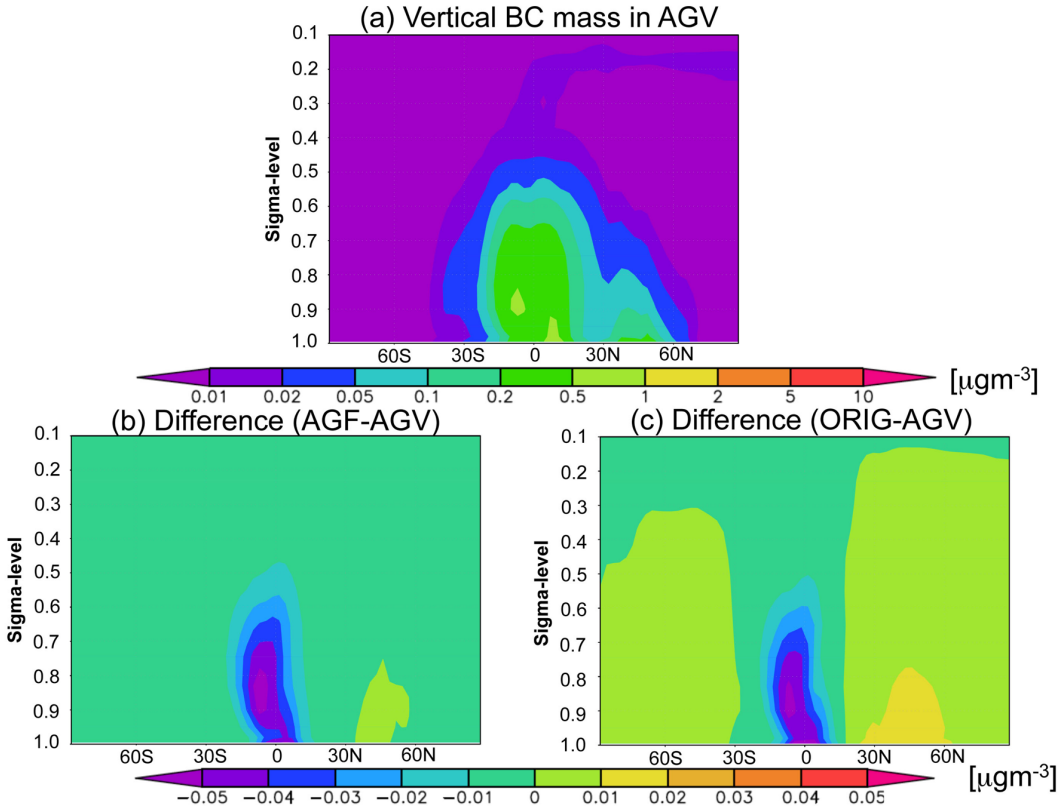

Fig. 5. Same as Figure 4, but for zonal mean BC mass concentration.

ACPD
12, 29801–29849, 2012

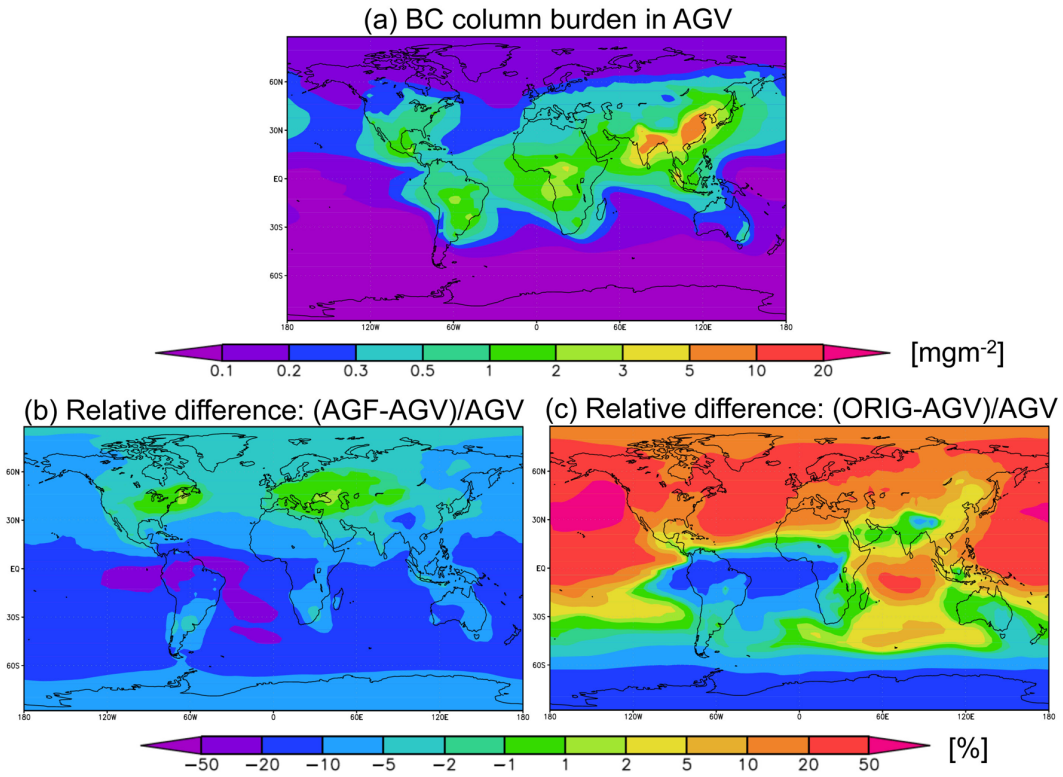

Fig. 6. Same as Figure 4, but for BC column burden.

ACPD
12, 29801–29849, 2012

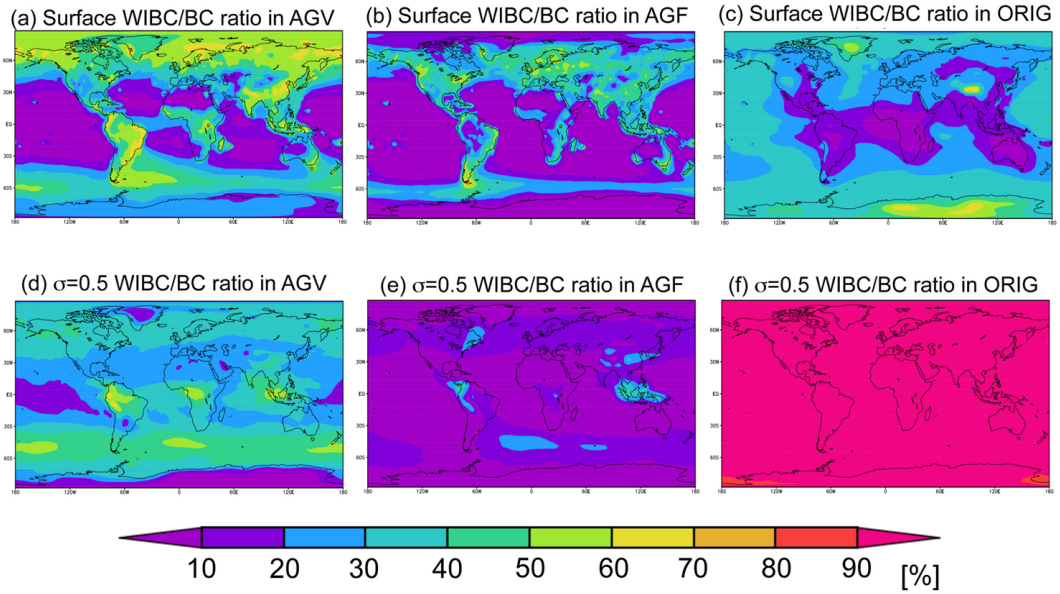

Fig. 7. Annual mean ratio of WIBC to total BC at the surface and the level of sigma 0.5.

ACPD
12, 29801–29849, 2012

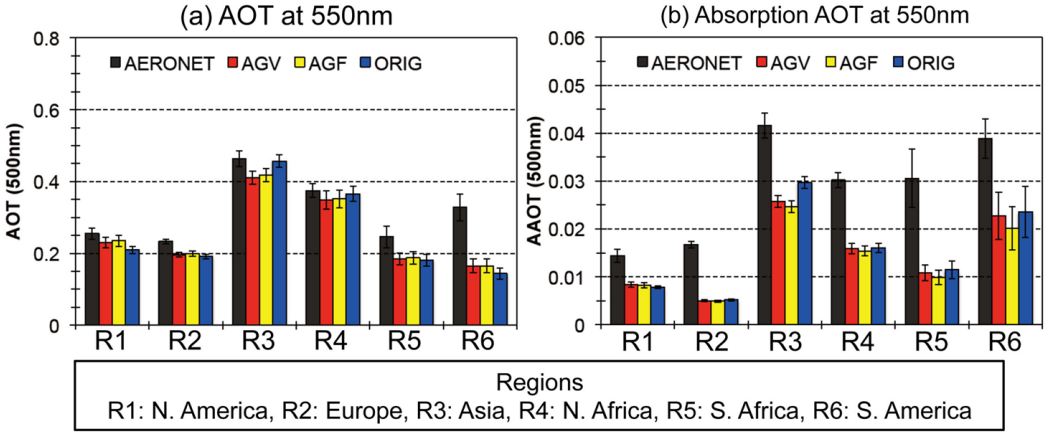

Fig. 8. Comparison of **(a)** AOT and **(b)** AAOT between the simulations and AERONET observation with a random var.

ACPD
12, 29801–29849, 2012

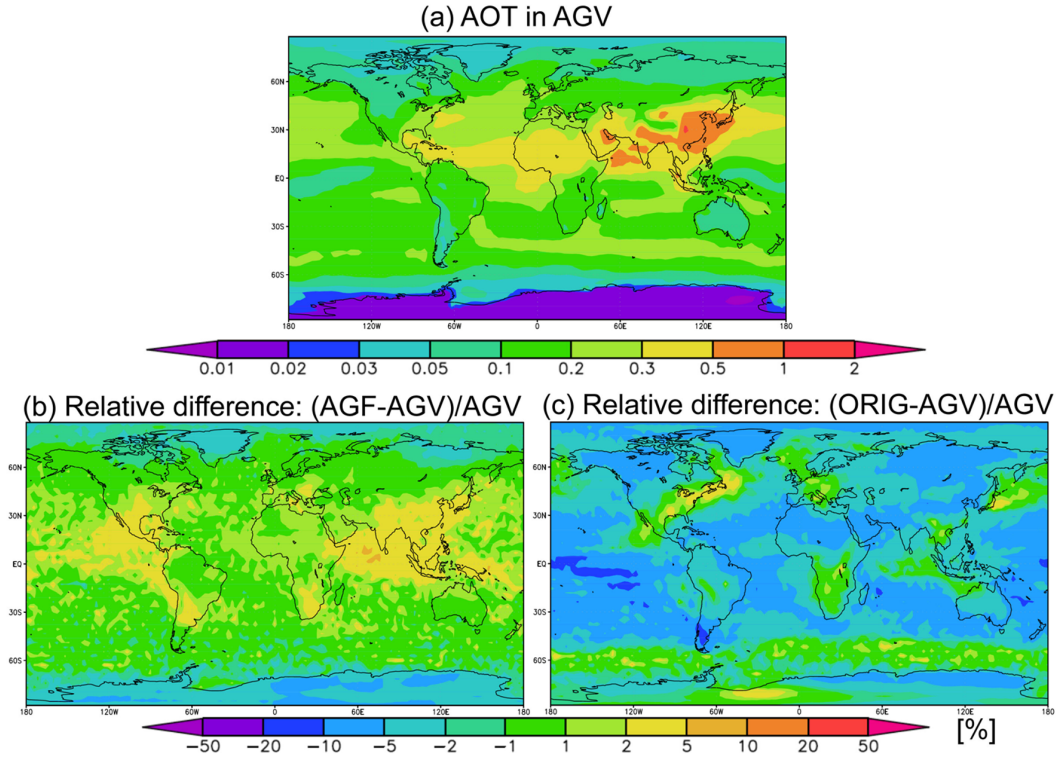

Fig. 9. Same as Figure 4, but for AOT.

ACPD
12, 29801–29849, 2012

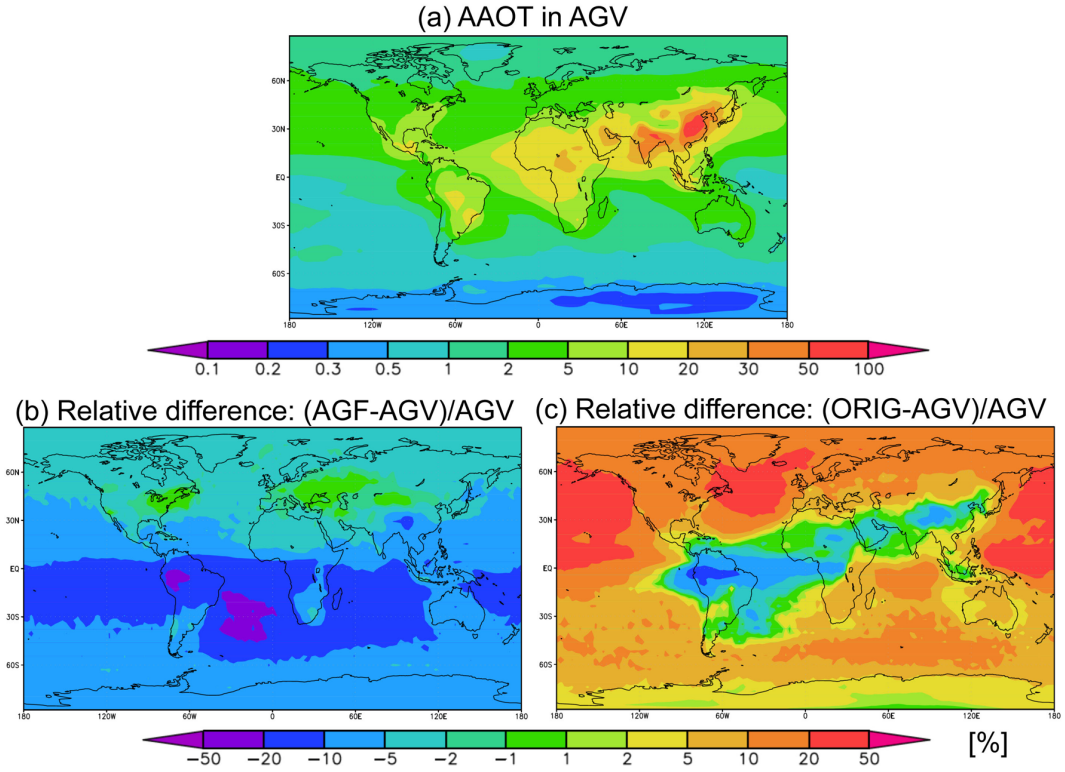

Fig. 10. Same as Figure 4, but for AAOT.

ACPD
12, 29801–29849, 2012

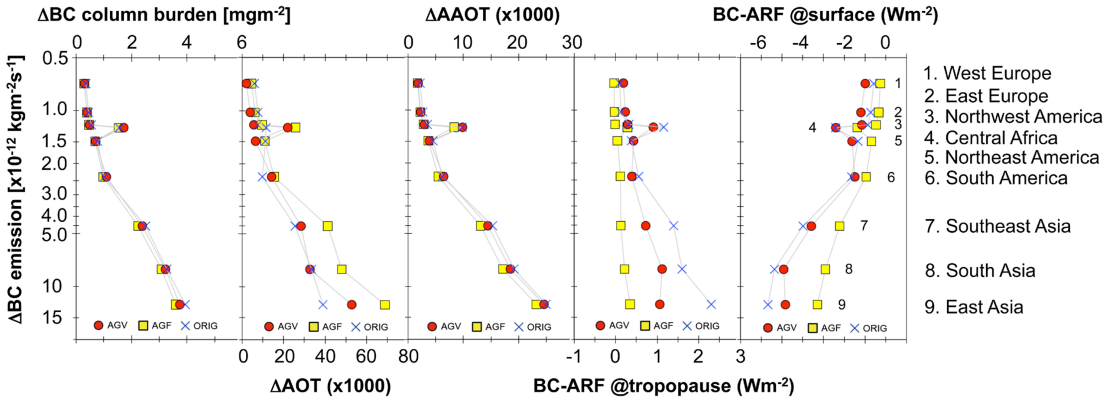

Fig. 11. Regional estimations of the annual mean relation between difference in BC emission and **(a)** BC column burden, **(b)** AOT, **(c)** AAOT, **(d)** ARF due to BC compound at the tropopause under all-sky conditions and **(e)** ARF due to BC compound at the surface under all-sky conditions, respectively. The regions are West Europe (15° W–20° E, 35–65° N), East Europe (20–55° E, 35–65° N), Northwest America (120–85° W, 15–55° N), Central Africa (20° W–20° E, 10° S–10° N), Northeast America (85–60° W, 15–55° N), South America (70–40° W, 40° S–0), Southeast Asia (90–120° E, 0–25° N), South Asia (60–90° E, 5–30° N), East Asia (100–140° E, 25–45° N).

ACPD
12, 29801–29849, 2012

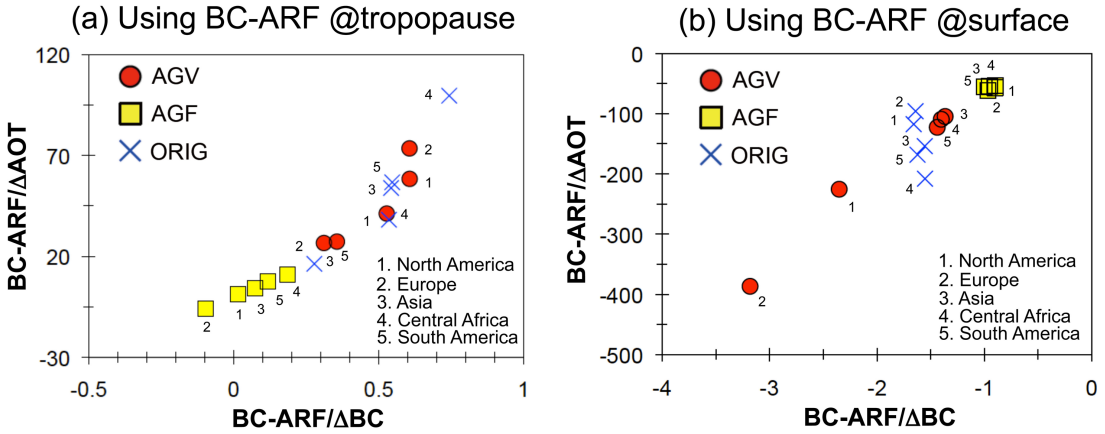

Fig. 12. Correlations between two different normalized efficiencies, (1) forcing efficiency (β_n) defined as a ratio of BC-ARF to a difference in AOT between experiments with/without BC aerosols, BC-ARF/ΔAOT, and (2) BC specific forcing efficiency (β_s) defined as, a ratio of BC-ARF to a difference in BC column burden between experiments with/without BC aerosols, BC-ARF/ΔBC, at the tropopause and surface in a regional average The regions are defined as those used in Fig. 11.

ACPD
12, 29801–29849, 2012